AFOSR-TR-95

0612

REPORT DOCUMENTATION PAGE

1. AGENCY USE ONLY (Leave blank)	2. REPORT DATE	3. REPORT TYPE AND DATES COVERED
	8/21/95	Final Technical 6/15/92 - 8/14/95

4. TITLE AND SUBTITLE

(U) Use of Maximum Entropy Principle as a Guide in Design of Spray Nozzles

5. FUNDING NUMBERS

PE - 61102F
PR - 2308
SA - BS
G - F49620-92-J-0389

6. AUTHOR(S)

Richard S. Tankin

7. PERFORMING ORGANIZATION NAME(S) AND ADDRESS(ES)

Northwestern University
333 Clark Street
Evanston, IL 60208

8. PERFORMING ORGANIZATION REPORT NUMBER

9. SPONSORING/MONITORING AGENCY NAME(S) AND ADDRESS(ES)

AFOSR/NA
110 Duncan Avenue, Suite B115
Bolling AFB DC 20332-0001

10. SPONSORING/MONITORING AGENCY REPORT NUMBER

11. SUPPLEMENTARY NOTES

12a. DISTRIBUTION/AVAILABILITY STATEMENT

Approved for public release; distribution is unlimited

12b. DISTRIBUTION CODE

13. ABSTRACT (Maximum 200 words)

The maximum entropy model predicted, under certain operating conditions, that a spray will have a bi-modal size distribution. Experiments were performed that verified this prediction. In seaching the literature, other researchers have observed bi-modal size distributions over limited range of operation. Their experimental results were compared with the calculated values and they agreed. Experiments were performed on the disentegration of a cylindrical liquid jet (Rayleigh problem). This flow results in a very strong bi-modal size distribution consisting of primary drops and satellite drops. The maximum entropy theory was modified to account for non-sphericity of the droplets. The computed size and velocity distributions (non-Gaussian) agreed with theory. Experiments were also performed on a heated cylindrical liquid jet. The maximum entropy theory was extended to include not only size and velocity distributions but also temperature distributions. There is agreement between theory and experiments.

14. SUBJECT TERMS	15. NUMBER OF PAGES
Sprays, maximum entropy principle, Rayleigh flow	44
	16. PRICE CODE

17. SECURITY CLASSIFICATION OF REPORT	18. SECURITY CLASSIFICATION OF THIS PAGE	19. SECURITY CLASSIFICATION OF ABSTRACT	20. LIMITATION OF ABSTRACT
Unclassified	Unclassified	Unclassified	UL

EXECUTIVE SUMMARY

The maximum entropy principle predicted a bi-modal size distribution, which was verified experimentally - for pressure atomizers and Rayleigh flow - as seen in Figures 1, 2 and 3. Experiments and theory were extended to include heat transfer for Rayleigh flow. A temperature distribution for the droplets (see Figure 4) as well as size and velocity distributions were obtained.

The following researchers were supported (in part) by this contract:

(1) Richard S. Tankin - Principal Investigator

(2) Long P. Chin - Research Scientist

(3) P. C. Hsing - Research Assistant

The following papers have been accepted for publication:

"Bi-modal Size Distributions Predicted by Maximum Entropy and Comparison with Experimental Measurements in Sprays," by Long P. Chin, Richard S. Tankin, T. Jackson. and J. Stutrud, G. Switzer. To appear in *Combustion Science and Technology*.

"Comparisons Between Experiments and Predictions Based on Maximum Entropy for the Breakup of a Cylindrical Liquid Jet," by L. P. Chin, P. C. Hsing, R. S. Tankin, and T. Jackson . To appear in *Atomization and Sprays*.

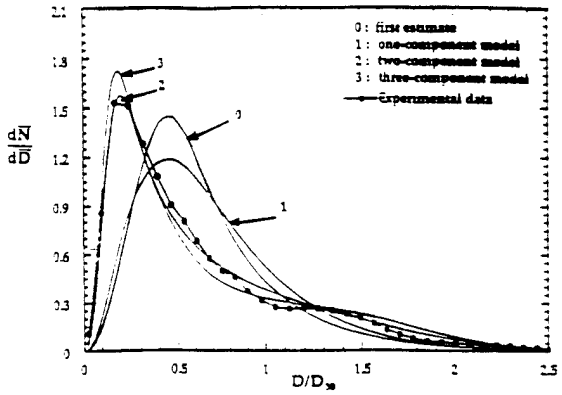

Figure 1. Comparison of droplet size distributions between experimental measurement and calculated results. In the three-component model the percentage of the third velocity component (tangential) in the total kinetic energy is 4%.

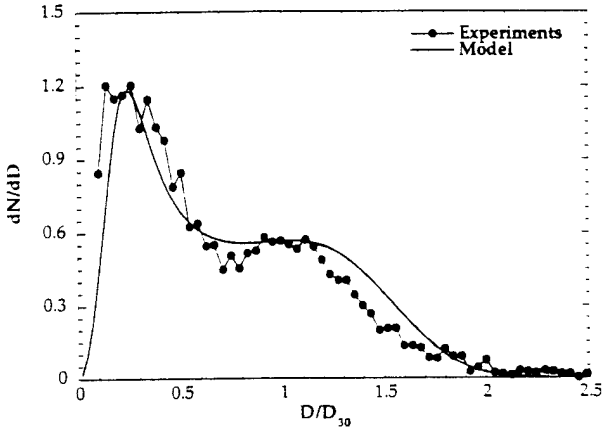

Figure 2. Comparison of bi-modal droplet size distributions between model and experiment (Gupta et al., 1986)

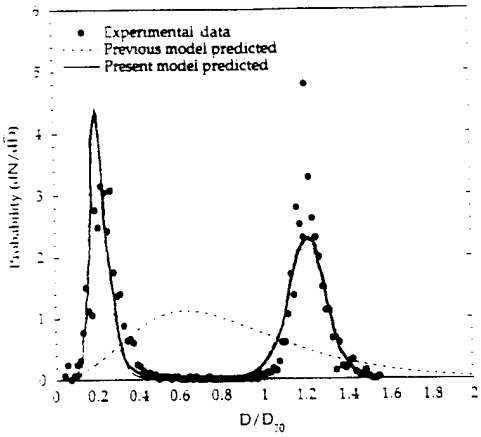

Figure 3. Comparison between experimental and predicted droplet size distributions.

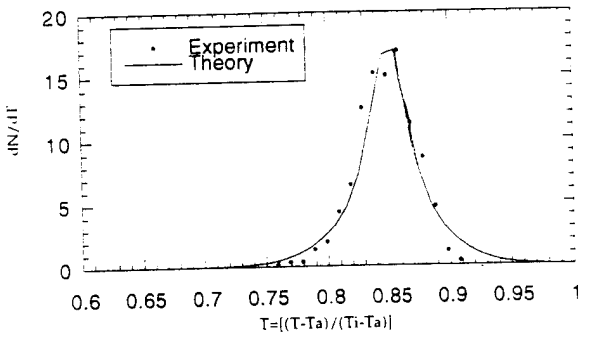

Figure 4. **Droplet temperature distribution of cylindrical liquid jet.**

INTRODUCTION

Sprays play an important role in the operation of combustion systems and can improve performance and reduce pollutant emission. The spray characteristics due to the atomization of liquid fuel, such as occurs in gas turbine engines, internal combustion engines, industrial furnaces, etc., have been the focus of research for many years. One aspect in the modeling of sprays is to understand the detailed information about the droplet distributions in size, velocity and temperature. Several famous droplet size distribution functions (Mugel and Evans [1951] and Tishkoff and Law [1977]) are widely used by many researchers and engineers. However, due to the complicated nature of sprays in various combustion systems, none of these functions can adequately describe all sprays.

In statistical mechanics, Jaynes'[1957] maximum entropy principle is a method of statistical inference to solve a probability problem when the information available is limited to some average quantities (constraints); such as, the mean, variance, etc. From this limited information, the most probable probability distribution will be the one that can maximize the Shannon entropy. Maximum entropy principle has been successfully applied in many problems arising out of several disciplines, e.g., thermodynamics, economics, business and finance, transportation, geography, fluid dynamics, image processing, etc. The basic concept and derivation of the maximum entropy principle can be found in several books (Levine and Tribus [1979], Kapur and Kesavan [1992]).

Recently, the maximum entropy principle has become a useful tool in the area of spray combustion to obtain droplet distributions. The diversity in the results is due to different choice of constraints imposed on sprays. A model with fewer constraints may simplify the problem as far as computations concerned, but may not be valid for the sprays in a complicated system. There are several examples of maximum entropy spray models developed since the mid-1980's: a Nukiyama-Tanasawa type model (Li and Tankin [1987]); one-velocity/combined energy model (Li and Tankin [1988], Li, Chin et al [1991]); a one-velocity/separate energy model (Sellens and Brzustowski[1985], Chin et al[1991]); and a two-velocity model (Sellens [1987], Sellens [1989]). These models

differ primarily by the number of droplet velocity components modeled and the energy flux (surface energy flux and kinetic energy flux) constraints imposed (combined or separate). All these models have been tested by comparing the calculated results with experimental data and agreement is reasonably good.

The previous models (Li et al [1991] and Chin et al [1991]) were modified in this study. In an earlier paper by Chin and Tankin [1991], bi-modal size distributions were predicted using the maximum entropy model, but no experimental observations were known by the authors, at the time, to corroborate this prediction. There is no model, prior to this, that is known by this author which predicts a bi-modal size distribution. Thus one of the purposes of this study was to compare the maximum entropy model with an experimentally determined bi-modal size distribution. Another purpose of this study was to determine the effects of heat transfer on droplet temperatures - that is a droplet temperature distribution.

This report will be divided into the following three sections:

(1) Bi-modal size distrubtion of a spray from a pressure atomizer

(2) Bi-mdal size distribution and velocity distribution of a spray from an isothermal cylindrical jet

(3) Size, velocity and, temperature distributions of a spray from a heated cylindrical jet.

In all of these sections experiments were performed and compared with theory.

I. BI-MODAL SIZE DISTRIBUTION FROM PRESSURIZED ATOMIZER

To extend MaxEnt method to more complicated spray systems, our previous models (Li, Chin, et al [1991], Chin, LaRose, et al [1991]) were modified. All three droplet velocity components for any coordinate system were included in the momentum flux and kinetic energy flux constraints. As a result, the previous models with fewer velocity components are special cases of this new and more general model. This more general model considers all three velocity components and is applicable to problems such as a spray nozzle where swirl is present. An important new discovery revealed by the model is that the size distribution may be bi-modal under certain operating conditions (Chin and

Tankin [1991]. To test this general model, particularly the bi-modal size predictions, a comparison was made between a set of experimental data obtained using a phase/Doppler particle analyzer (PDPA) and the calculated results.

The nozzle used in these experiments was an Allison hollow cone, non-swirl spray nozzle having a 90° spray angle. A spray of water issues into a quiescent, saturated air environment at 295°K at a flow rate of $2.75 \times 10^{-6} m^3/s$ (2.5 gallons/hr). The water exiting the nozzle forms a liquid sheet, hollow cone in shape, which breaks up into ligaments and droplets. The ligaments breakup into droplets further downstream. It is desirable to measure the spray as close as possible to the sheet break-up region — but downstream of the ligament region. Measurements beyond this point will be influenced by local gas aerodynamics and complicate the comparison with calculations. Droplets are sized with an Aerometrics, Inc. two-color, four-beam PDPA.

A droplet size distribution is constructed from the individual point measurements, weighting each measurement by their time of collection and the ratio of their optical probe area to the ring area represented at that location. Droplet size is normalized by the mass mean diameter, D_{30}, which was determined from measurements to be 81.43 microns. The resulting experimentally determined probability size distribution is shown in Fig. 1. It should be noted that there is evidence of a bi-modal size distribution - although not a strong bi-modal distribution. One peak occurs at $\overline{D} \approx 0.2$ and the second peak at $\overline{D} \approx 1.3$. A physical explanation for the origin of these peaks is as follows: There are two main sources for the droplets in this spray — the droplets that form from the ligaments and those that form from the thin sheet of liquid that lies between the ligaments at breakup. The ligaments breakup via Rayleigh's capillary instability and form the larger droplets associated with those centered around $\overline{D} \approx 1.3$ (in Fig. 1). The droplets from the thin sheet are associated with those centered around $\overline{D} \approx 0.2$. It should be mentioned that such a bimodal size distribution is not typical for this nozzle. However when the nozzle in this study was operated at low flow rates - 2.75×10^{-6} m^3/s - a bimodal size distribution appeared. That was the motivation for operating this nozzle at such low flow rates, since one of the goals was to verify the validity of the MaxEnt model which predicts a bimodal size distribution at particular operating conditions. Also shown in Fig. 1 are the computed results for a one component velocity model, two-component velocity model and a three component velocity model.

The three component velocity model exhibits a bimodal shape that is in reasonable agreement with the experiments.

The influence of the small velocity component (tangential component in this case) on the droplet size distribution will be examined. Figure 2 shows a set of droplet size distributions obtained by assigning different values of $\overline{M}_\theta$ (the tangential momentum flux) while the other constraints are not changed. Each droplet size distribution in Fig. 2 is characterized by the ratio of the kinetic energy flux of the tangential component in the total kinetic energy flux. It is noted that the bi-modal distribution can be enhanced by increasing the magnitude of the third velocity (tangential) component. Curve "2" (4%) in Fig. 2 corresponds to curve "3" (three-component model) in Fig. 1. 4% of the total kinetic energy amounts to a tangential velocity of only 0.35m/sec. This is reasonable from values of the tangential velocity that were determined experimentally.

Presser et al [1990] and Gulder [1990] obtained experimentally significantly strong bi-modal size distributions. Presser et al represented their bi-modal size distribution function by the sum of two mono-modal log-normal distribution functions with a weighing factor. To properly fit the data, they had to determine five fitting parameters. Cary Presser has been kind enough to provide us with his experimental data that he published with Gupta, Santoro, and Semerjian [1986]. This experimental data is for a swirl nozzle and exhibits a strong bi-modal size distribution. The computed size distribution curve using the procedures presented in this study agreed reasonably well with their experiments as seen in Figure 3. Note that the axial velocity in this experiment is relatively small for a pressure atomizing nozzle, and that the spray has swirl. In our experiments, a bi-modal distribution was only observed at low flow rates (low U_o) and the computations predict that increasing the tangential velocity component (swirl) strengthens the bi-modal distribution (see Figure 2). It has been shown that the maximum entropy principle will yield directly a bi-modal size distribution for a particular set of spray quantities. Prior to this study, the maximum entropy principle has successfully yielded skewed mono-modal and uniform (approximating a delta function) distributions (see Li et al [1991] and Chin et al [1991] respectively). Now it has been shown that the maximum entropy principle successfully predicts bi-modal size distributions.

II. BI-MODAL SIZE DISTRIBUTION - RAYLEIGH PROBLEM

The process of producing droplets by the breakup of a cylindrical liquid jet is commonly called Rayleigh breakup (Rayleigh [1879 & 1882]). The use of a stimulated mechanism (forcing function) has been widely employed to obtain uniform droplets; that can be represented by $\delta(D-D_0)\delta(U-U_0)$--a coupled delta function where D_0 denotes uniform droplet size and U_0 denotes uniform droplet velocity. Such droplets are essential in calibrating spray sizing instruments and in studying the fundamental aspects of spray evaporation and combustion. In general, a stream of droplets having uniform size is difficult to achieve without external stimulation, even when experiments are carefully conducted in a vibration isolated environment. Such a jet, as a result of nonlinear instability, frequently has a propensity to produce relatively small "satellite" droplets interspersed among the main large droplets (Bogy [1979]). The existence and behavior of these satellite droplets depends on the initial flow conditions and the physical properties of the liquid jet.

The maximum entropy principle has been used successfully to study the droplet size and velocity distributions for non-stimulated cylindrical water jets without satellite droplets (Chin, LaRose et al [1991]). Unforced disturbances and complicated nonlinear breakup mechanisms produced a stream of droplets that deviated from the ideal (deterministic) uniform distributions in size and velocity. The present study extends the use of the maximum entropy principle to a stream of primary and satellite droplets, whose size and velocity distributions are not deterministic; and thus, are described by probability distribution functions.

In a recent paper by van der Geld and Vermeer [1994], a size distribution function of a spray having satellite drops was derived using maximum entropy formalism. However in their derivation, the size distribution for the primary droplets is assumed to be Gaussian. Maximum entropy theory was used to obtain the size distribution for the satellite drops; the final distribution is a composite distribution. In the study presented here, no assumption was made *a priori* with regard to either the primary or satellite droplet distributions. A single probability distribution function, not a composite type, was obtained that incorporates both primary and satellite drops.

The goal of this study was to examine a flow system having a strong bi-modal size distribution. Rayleigh breakup of a cylindrical liquid jet with satellite droplets was an ideal candidate. This is essentially a simple spray, which however has complex size and velocity distributions. Stimulating the flow (piezoelectrically, acoustically, etc.) can produce very reproducible flows having a bi-modal size distribution that incorporates essentially two delta functions--one for the primary drops and another for the satellite drops. These flows have been studied by conventional deterministic approach--linear or non-linear stability analyses Yuen[1968],Goedde and Yuen [1970], Nayfeh [1970], Rutland and Jameson [1970], Lafrance [1974]. However a Rayleigh liquid jet that is not externally stimulated produces droplets that vary in size and velocity; and thus are described by probability distribution functions which are amenable to the maximum entropy approach used in this study.

A schematic diagram of the apparatus used to study the evolution of droplets is illustrated in Fig. 4. A compressed air supply forces the water from a reservoir through a filter to the nozzle assembly. The nozzle assembly, which is positioned vertical with the fluid exiting downward, has an inner diameter of about 2.54 cm. Inside the nozzle assembly are three fine stainless steel screens; above these screens are several layers of glass beads that are 0.47 cm in diameter. Thus non-uniformity and rotation of the liquid flow are removed. The orifice in the nozzle assembly consists of a sapphire orifice with a 0.08 cm hole. The flow is accurately controlled by a needle valve placed between the pressure source and the pressurized water tank, and a ball valve placed upstream of the water filter. The operating pressure drop across the nozzle assembly for this test was 7.6 kPa yielding a volumetric flow rate of 2 ml/sec. The volumetric flow rate was measured by weighing the total mass of water collected over a selected interval of time.

A Kodak image analyzer was used to take pictures of the water droplets. The water issues from the nozzle assembly as a liquid column. This liquid column breaks up into droplets about 10 cm downstream from the orifice. The motion analyzer was set up about 10 cm downstream of the orifice to record the droplet formation in the vicinity of the breakup region. A strobe light having a very short pulse duration (less than a microsecond) was used to provide illumination of the droplets. The strobe flash is of sufficiently short exposure time to provide images of the droplets with little distortion due to droplet motion--

which is particularly important for measuring the size of the satellite droplets. The illuminating strobe light and the image camera were both triggered by a synchronized signal from the image processor. The images "seen" by the camera were enlarged 10 fold by a microscope.

As stated earlier, measurements must be made on droplets near the breakup region, otherwise many of the satellite drops may have coalesced with primary (large) drops. Due to the influence of inherent instabilities from various sources, the breakup plane is not fixed in space and was found to fluctuate about $\pm$ 1.5 cm. This fluctuation was more than the view area seen through the microscope. Thus, some of the images had only a cylindrical column of water with no droplets (image is upstream of the breakup plane); whereas some of the other images have satellite droplets on the verge of coalescing with the primary drop. Possibly some satellite drops may have already coalesced with primary drops and we missed counting them. In the experiment, a total of 1017 primary droplets and 877 satellite droplets were counted and analyzed. Thus, the measured number ratio of primary droplets to satellite droplets at breakup is 1.16.

Figure 5 shows the images taken at a framing rate of 1500 pictures per second. In these images the droplets are traveling from left to right. Both primary and satellite droplets appear. In Fig. 5a, no satellite drop is seen between droplets labeled "b" and "c" in the first frame nor between "e" and "d" of the third frame. In Fig. 5b, the satellite drop between droplets "b" and "c" in the first frame is about to coalesce with droplet "b" in the second frame. There are some instances where there are two satellite drops between the two primary drops.

The satellite drops are nearly spherical in shape; on the other hand, the primary drops are relatively large in size, but are far from spherical. It was necessary to characterize the drop sizes by an effective diameter. It was assumed that all the droplets are ellipsoidal in shape (either prolate or oblate spheriods) with their axes of symmetry along the flow direction (vertical in experiments and horizontal in images shown in Figure 5). By measuring the major and minor axes of droplet, the volume of the droplet was calculated. The diameter of a sphere with an equivalent volume was obtained and its diameter was defined as the effective diameter for the droplet. The accuracy of the measurements of the major

and minor axes for an individual drop is 22.5μm.The standard deviation of the mean was computed from fifty such measurements on a typical satellite drop and primary drop - the values were 2.2 μm (mean diameter is 0.32 mm) for the satellite drop and 3.5 μm (mean diameter is 1.35 mm) for the primary drop. Thus the measured effective diameters of the droplets are a good representation of the droplet sizes. There may be some question concerning their accuracy, but they do not have to be any more accurate because the effective diameters are non-dimensionalized with the mass mean diameter (D_{30}); and D_{30} is computed based on the measured effective diameters. As a further verification of the measured diameters of the non-spherical primary drops, measurements were made far downstream (approximately 50 cm from nozzle). At this location (see Fig. 6) the primary drops are round and their diameters (equal to effective diameters) can be measured directly (the increase in volume due to coalescence with a satellite drop is negligible). Although there may be coalescence between some primary drops at 50 cm from the nozzle, the diameters at the peak of the distribution curves in both cases (at 10 and 50 cm from the nozzle) agree at 1.37 mm.

The measured droplet size distribution is shown in Fig. 7. Two peaks exist; one for the satellite droplets and the other for the primary droplets. The amplitude of the peak for the primary droplets is slightly larger than that for the satellite droplets. As mentioned earlier, a few satellite drops may not have been counted because of coalescence prior to the images under consideration. Using the measured effective diameters, D_{30} was calculated to be 1.1 mm. From the recorded images similar to those shown in Fig. 5, the velocities of the droplets at breakup plane were measured. The mean velocity of the droplets at the breakup region was found to be 4.15 m/sec. An experimentally measured velocity distribution will be presented later and compared with the predicted velocity distribution function.

Detailed formulation and derivation of the maximum entropy principle, as presented here, have been published Li and Tankin [1987], Li, Chin et al [1990] and Chin, LaRose et al [1991]. However, there is one significant modification for the model presented here. The previously presented model is derived based on the assumption that the droplets are spherical. In the present study, the satellite drops in most instances are nearly spherical; however the primary (large) drops

are far from spherical. Their actual shapes, which vary from frame to frame, are complicated and difficult, if not impossible, to describe mathematically. To account for these non-spherical shapes, two new constraints are introduced-- one is related to surface/volume ratio of small droplets and the other is related to the non-sphericity of large droplets:

(1). Since the small drops (satellite) are nearly spherical, the area/volume ratio of a satellite drop is equal to $6/D$ (D is the diameter of droplet). Therefore, it was assumed in this model that the mean area/volume ratio for the group of small satellite droplets varies inversely with $\overline{D}$ (D/D_{30}). This constraint is dominated by small droplets ($\overline{D} << 1$).

(2). It is known that the surface to volume ratio for a sphere is smaller than that of any other shape having the same volume. From the examination of experimental data, it is observed that the larger the drops, the greater the deviation from spherical shape. A mathematical model for large droplets based on experimental observations can be established by describing the large droplet as a prolate spheroid having a major axis "a" and a minor axis "b." The surface area for a prolate spheroid (A_e) is greater than the surface area of a sphere (A_s) having the same volume. The greater the ratio of the major axis to the minor axis, the greater the ratio A_e/A_s. If we assume that the ratio between major axis and minor axis follows this relationship, $a/b = \delta D_{eq}^{\beta}$, as the droplet size increases, then it is found that the ratio A_e/A_s is proportional to D_{eq} as shown in Fig. 8. D_{eq} is defined as the diameter of a sphere having the same volume as the prolate spheroid. The proportionality between A_e/A_s and D_{eq} depends on the values of δ and β, which indicate the degree of deviation for the shape of droplet from a sphere. It is clearly seen in Fig. 8 that the curves are approximately linear with D_{eq}. Therefore, as a second constraint, we assumed that A_e/A_s varies linearly with $\overline{D}$ ($\overline{D} = D_{eq}/D_{30}$). This constraint is dominated by large (primary) droplets.

The solid line in Fig. 7 shows the predicted size distribution where the two source terms which account for non-sphericity are used. One can see there is reasonably good agreement between the experimental size distribution and the computed size distribution. A predicted size distribution having the same source terms without the non-sphericity constraints is also shown in Fig. 7. This plot is not bi-modal and does not agree with the experimental data. Thus to obtain a bi-

modal size distribution for a Rayleigh breakup of a cylindrical jet using maximum entropy principle, one must introduce constraints which account for non-sphericity in the drops.

In Fig. 9 are plots of the experimental and computed velocity distributions obtained from the probability density function. Again, it is seen that there is reasonably good agreement between experimental and computed velocity distributions. It should be noted that the velocity distribution for both the experimental and computed curves are broad at the base and merge rather abruptly into a rather narrow distribution which is not a Gaussian shape. To further explain this non-Gaussian shape, the joint probability distribution function, $f(\overline{D},\overline{U})$, is plotted in Fig. 10. The velocity distributions for the satellite drops and the primary drops are Gaussian individually, but the integrated velocity distribution is a non-Gaussian distribution. Fig. 10 shows that the satellite drops have a much broader velocity distribution than the primary drops. Physically, one would expect a broader velocity distribution for the satellite drops because their velocity variance depends to a large extent on where the ligament separation first occurs--on the fore side of the primary drop (giving the satellite a higher velocity) or on the aft side of the primary drop (giving the satellite a lower velocity). Thus, the maximum entropy solution predicts a velocity distribution that accounts for the effect of ligament separation without specifically considering this in the formulation of the problem. This illustrates the point that the detailed physical processes involving the transition from one equilibrium state to another equilibrium state play no role in the maximum entropy approach.

A question arises: What would happen if the constraints involving non-sphericity were introduced in the formulation of a pressure atomizer experiment[8] where the measured size distribution is not bi-modal? Figure 11 shows the predicted droplet size distribution (labeled "Model A") presented in the paper by Li, Chin et al [1990] without the non-sphericity constraints. The curve labeled "Model B" is a plot where the non-sphericity constraints.(the other constraints in both models are kept the same) were introduced. Even though non-sphericity constraints were introduced, there is no bi-modal size distribution ("Model B")--it remains skewed monomodal. Thus the introduction of the non-sphericity constraints do not necessarily result in a bi-modal size distribution. A bi-modal size distribution depends on the other constraints (involving

conservation of mass, momentum, surface energy and kinetic energy) as well. Rayleigh breakup of a cylindrical liquid jet without satellites was also examined (Chin, LaRose et al [1991]). This system results in a distribution which is uniform in size and velocity. Adding non-sphericity constraints in the maximum energy formulation, results in droplet sizes (and velocities) which are uniform--not exhibiting any bi-modal shape. In summary, the occurence of a bi-modal size distribution depends on the entire set of constraints imposed--not just the introduction of non-sphericity constraints.

III TEMPERATURE DISTRIBUTION IN CYLINDRICAL JET

The experimental setup of the droplet temperature measurements is illustrated schematically in Fig. 12. A cylindrical liquid jet of higher temperature than the surroundings is directed vetically downward from a converging nozzle. The diameter of the nozzle at the exit is 2.16 mm. At the breakup point, the liquid jet breaks up into droplets of different sizes. An infrared photo sensor containing an emitter and detector is positioned 25 mm below the breakup point. A fast-response micro-miniature thermocouple is attached 3 mm below the horizontal line of sight of the infrared photo sensor. Normal tap water is heated to a high temperature and stored in a reservoir. The flow rate of the liquid jet, which is gravity driven, is fine tuned by a valve located in the flow line between the reservoir and the converging nozzle. Hot water flows from the reservoir, through the control valve, past the static pressure gage, and into the converging nozzle. The heated water exits the nozzle as a cylindrical liquid jet at temperature T_i and velocity v_i into the quiescent air environment which is at temperature T_a.

Several tests are performed, each having about 500 or more valid data points for the droplet temperature measurements (as well as the size and velocity measurements). The whole process - acquiring the data (about 2 seconds for each data file) and creating the data files - takes less than 30 seconds for each experiment. The initial temperature of the liquid jet at the nozzle exit is measured by a thermocouple and averaged over 10 seconds. This exit temperature fluctuates $\pm$0.2°C over the period of a test.

Four different initial condions - temperature and velocity at the nozzle exit - were used to determine their effects on the breakup length; and the velocity, size, and temperature distributions. These initial conditions are indicated in Table 1.

Since there is no external disturbance imposed on the system, the breakup point tends to oscillate over a distance of 5-10 mm. This oscillation creates some difficulty in determining the precise value of the breakup length. From several photographs, an average value for the breakup length is obtained. It is found in this study - over the range of experiments performed - that the breakup length varies linearly with the initial velocity at the nozzle exit. This is seen in Figure 13. Thus, the time that an element of fluid takes from traversing from the nozzle exit to the breakup point is constant for the range of experiments in this study.

A chromel-alumel type thermocouple having a micro, disk-shaped tip configuration was used. The micro-disk thermocouple is exposed; thus, resulting in a unit having a fast response time (0.001 second) in water. Figure 14 is a schematic drawing showing the relative position of the micro thermocouple to the infrared photo sensor with a train of droplets moving through the test section. The droplet is first detected by the photo sensor and then its temperaure is measured by the micro thermocouple as the droplet impinges on the thermocouple. Thus, there is a signal lag in the voltage signals from the photo sensor and the thermocouple.

Figure 15 shows the droplets impinging on the thermocouple. It is seen that as the primary drop impinges on the thermocouple, it becomes distorted and no longer maintains its original ellipsoidal shape. As the drop leaves the thermocouple, a tail of liquid remains attached to the thermocouple for a period of time. This situation also exists for the satellite drops as seen in Figure 16(b). Thus the thermocouple remains wet after the droplet has passed the thermocouple and the next drop impinges on the thermocouple. Therefore the thermocouple always remains wet and never reaches room temperature. Fortunately one is interested in the maximum temperature recorded by the thermocouple which is representative of the droplet temperature. It is not necessary to measure the room temperature between each drop.

The photo sensor is designed so that the voltage output is inversely proportional to the infrared light intensity falling on the detector. A drop passing through the line of sight of the photo detector acts as a lens. If the droplet is perfectly aligned so that the center of the drops passes through the line of sight of the photo detector, then there will be two peaks and a trough as voltage outputs. As the droplet first enters the line of sight, it deflects light from the detector

(voltage is inversely proportional to intensity) - thus yielding a peak voltage. The same situation occure when the droplet leaves the line of sight. If the droplet is axially symmetric - which it is in this case - the two peaks will be the same magnitude. When the center of the droplet crosses the line of sight, the light is focused on the detector, yielding a trough in the voltage output. This is clearly demonstrated in Figure 17. Two time constants are present in this problem - one when the droplet impinges on the thermocouple, and the other as the droplet leaves the thermocouple. These two time constants are quite different. In leaving the thermocouple, the droplet has a tail that remains attached for a significant period of time. Both of these time constants were estimated from the experimental data. The heating time constant (measuring droplet temperature) is found to be 0.9 millisecond and the cooling time constant (measuring air temperature) is 22.5 millisecond. The measured heating time constant of 0.9 milliseconds compares favorably with the computed value of 0.6milliseconds

In the manner described, one can identify the droplets and thus measure their temperature. This is necessary because unlike the records shown in Figure 17, the droplets in the tests under consideration will be generated at a rate of several hundred drops per second.

For the droplet temperature measurements shown in Fig. 18, the initial temperature of the liquid jet at the nozzle exit is 38.6 °C and the surrounding air temperature is 20.1 °C. The volume flow rate for this test is 1.56 ml/sec which yields an initial velocity equal to 0.43 m/sec at the nozzle exit. This velocity can be substituted into the empirical formula listed in Fig. 13 to calculate the breakup length. For these initial conditions, the breakup length is 9.6 cm. The temperature signal from the thermocouple and voltage signal from the photo sensor are sampled at a rate of 1 kHz and recorded simultaneously into a 486 PC. The local maximum corresponds to the droplet temperature, which is when the droplet leaves the thermocouple. The results shown in Fig. 19 were obtained under the following conditions: The temperature at the nozzle exit equals 37.6 °C, the surrounding air temperature (Tair) equals 20. °C, the breakup length is 10 cm, and the volume flow rate is 1.48 ml/sec. Both the experimental raw data and the non-dimensionalized droplet temperature distribution are presented.

The non-dimensionalized mean temperatures for case 3 and case 4 are about the same (see Figure 20) even though their initial temperatures at the

nozzle exit are quite different (14 °C). This situation also occurs for case 1 and case 2. The manner in which the temperature is non-dimensionalized ($T_i - T_a$), one would expect the non-dimensionalized mean temperature to be a weak function of the initial temperature at nozzle exit.

The technique for measuring of droplet size and velocity was similar to that used on the unheated cylindrical jet described in Section II. Both droplet size and velocity measurements can be accomplished at the same time because they share the same experimental imaging data. Once the experimental images are recorded by a high-speed camera and saved in a special video high speed imaging system, the experimental images can be transferred into image files and saved in the computer (Macintosh Quadra 700). Figure 21 shows droplets recorded at a framing rate of 375 pictures per second - at a position 125 mm below the nozzle exit. The initial temperature of the cylindrical liquid jet at the nozzle exit is 38.6 °C (18.6 °C higher than the ambient air temperature) and the volumetric flow rate is 1.55 ml/sec. The droplets in Fig. 21 are traveling from left to right. There are only 5 droplets observed in frames (a) to (i) in Fig. 21. One can see that the larger droplets tend to oscillate more vigorously than the smaller droplets.

The image files saved in computer are then be analyzed by using a drafting software package to extract the droplet size and velocity information. As shown in Fig. 22, the process of determining droplet size and velocity is very straight forward but tedious, since each droplet has to be measured manually. The droplet size measurement is achieved by assuming that the droplets are either axially-symmetry ellipsoids or oblate spheroids. This requires measurement of the major and minor axes. If the droplet appears in more than one picture, which is usually the case (see Fig. 21 and Fig. 22), the one with the shape closest to a sphere is selected to calculate the volume of the droplet. From the volume measurement, the diameter of a sphere having the same volume is used in determining the droplet diameter (size).

The droplet velocity is determined by measuring the distance between the mass center of a particular drop from one frame to another (see Fig. 22). Although there is human error in this method, by measuring the velocity of a large number of droplets random errors are reduced, In addition, the measured results are presented in non-dimensional form, which may further reduce errors.

In Fig. 3.15, the size and velocity of droplet "A" is determined to be 2.84 mm and its velocity is 1.35 m/sec repectively.

The experimental droplet size distributions, for various experimental conditions, are presented in Fig. 23. Over the range of initial conditions in this study, the non-dimensionalized droplet size distributions are very similar.

The experimental droplet velocity distributions for various initial conditions are presented in Fig. 24. The abscissa is the non-dimensionalized droplet velocity - scaled from 2 to 8 - and the ordinate is the number probability of the droplet velocity distribution. The droplet velocity distributions for case 1 and case 2 are very similar and have a peak value of 2.5 at $\overline{v}$ equal to 3.6; case 3 and case 4 are also very similar and have a peak value of about 1.7 at $\overline{v}$ equal to 5.1. The initial temperature of the liquid jet at the nozzle exit has little influence on the final droplet velocity distribution. It appears the breakup length is the dominant influence on the velocity distribution. This is expected because the breakup length effects both the potential energy and the areodynamic drag on the column of fluid - which, in turn, effect the droplet velocity.

The maximum entropy principle is now being used to predict these distributions - velocity, size and temperature. The preliminary results agree with experiments as seen in Figure 25 which is a plot of the temperature distribution. When the imposed constraints are further examined and justified, these results will be submitted for publication.

CONCLUSIONS

The maximum entropy principle provides a very robust technique for determining size distributions, velocity distributions and temperature distributions in sprays. Depending on the source terms (which are related to the initial conditions at the nozzle exit and the ambient conditions), the size distribution may be skewed mono-modal, bi-modal or delta functions (uniform size). This has been demostrated in this study.

REFERENCES:

Bogy, D. B. (1979). Drop Formation in a Circular Liquid Jet, *Ann. Rev. Fluid Mech.*, Vol. **11.**

Chin, L. P., LaRose, P. G., Tankin, R. S., Jackson, T., Stutrud, J., and Switzer, G.(1991). Droplet distributions from the breakup of a cylindrical liquid jet.

Physics of Fluids **A**, **3**(8): pp. 1897-1906.

Chin, L. P. and Tankin, R. S.(1991). Theoretical prediction of droplet distributions in sprays based on maximum entropy theory. HTD, *Winter Annual Meeting ASME*, pp. 1-10.

Goedde, E. F. and Yuen, M. C. (1970). Experiments on Liquid Jet Instability, *Journal of Fluid Mechanics*, Vol. **40**, p.495.

Gulder, O. L. (1990). Multiple scattering effects in dense spray sizing by laser diffraction. *Aerosol Science and Technology*, **12**: pp. 570-577.

Jackson, T. A.(1990). Liquid particle size measurement techniques. *"Liquid Particle Size Measurement Technique,"* ASTM, **II**: p. 151.

Jaynes, E. T.(1957). Information theory and statistical mechanics, I and II. *Physical Review,* **106**: pp. 620-630, and **108**: pp. 171-190.

Kapur, J. N. and Kesavan, H. K.(1992). *Entropy Optimization Principles with Applications*, Academic Press, Inc., San Diego, California.

Lafrance, P. (1974). Nonlinear Breakup of a Laminar Jet, *Physics of Fluids*, Vol. **17**, p.1913.

Lee, S. Y. and Tankin, R. S.(1984). A study of liquid spray (ware) in a non-condensable environment. *Int. J. Heat and Mass Transfer*, **27**: pp. 351-361.

Levine, R. D. and Tribus, M.(1979). *The Maximum Entropy Formalism*, MIT Press, Cambridge, Mass.

Li, X. and Tankin, R. S.(1987). Droplet size distribution:A derivation of a Nukiyama-Tanasawa type distribution function. *Combustion Science and Technology*, **56**: pp.65-76.

Li, X. and Tankin, R. S. (1988). Derivation of droplet size distribution in sprays using information theory. *Combustion Science and Technology*, **60**: pp.345-357.

Li, X., Chin, L. P., Tankin, R. S., Jackson, T., Stutrud, J., and Switzer, G.(1991). Comparison between experiments and predictions based on maximum entropy for sprays from a pressure atomizer. *Combustion and Flame*, **86**: pp. 73-89.

Mugele, R. and Evans, H. D.(1951). Droplet distribution in sprays. *Industrial Engineering Chemistry*, **43**: pp.1317-1324.

Nayfeh, A. H. (1970). Nonlinear Stability of a Liquid Jet, *Physics of Fluids*, Vol. **13.** p.841.

Presser, C., Gupta, A. K., Dobbins, A., and Semerjian, H. G.(1990). Influence of size distribution on droplet mean diameter obtained by ensemble light scattering. *Liquid Particle Size Measurement Technique* - ASTM, **II**: pp. 93-111.

Presser, C., Gupta, A.K., Santoro, R.J., and Semerjian, H.G. (1986). Laser diagnostics for characterization of fuel sprays. *Proceedings ICALEO*, **58**.

Rayleigh, L (1879). On the Instability of Jets. *Proc. London Math. Soc.*, Vol. **10**.

Rayleigh, L. (1882). Further Observations upon Liquid Jets, *Proc. R. Soc. London*, Vol. **34**.

Rutland, D.F. and Jameson, G.J. (1970). Theoretical Prediction of the Size of Drops Formed i *Sci.*, Vol. **25**, p.1689.

Sellens, R. W. and Brzustowski, T. A.(1985). A prediction of the drop size distribution in a spray from first principle. *Atomization and Spray Technology*, **1**: pp. 89-102.

Sellens, R. W. (1987), Ph. D. thesis, University of Waterloo.

Sellens, R. W.(1989). Prediction of the drop size and velocity distributions in a spray, based on the maximum entropy principle. *Part. Part. Syst. Charact.*, **6**: pp. 17-27.

Shannon, C. E.(1948). A mathematical theory of communication. *Bell System Tech. J.*, **27**: pp. 379-423, 623-659.

Tishkoff, J. M. and Law, C. K.(1977). Application of a class of distribution functions to drop-size data by logarithemic leastsquares technique. *Journal of Engineering for Power*, **99**: pp. 684-688.

van der Geld, C.W.M. and Vermeer, H. (1994). Prediction of Droplet Size Distributions in Sprays Using the Maximum Entropy Formalism: the Effect of Satellite Formation, *Int. J. Multiphase Flow*, Vol. **20**, pp.363-381.

Yuen, M. C. (1968). Nonlinear Capillary Instability of a Liquid Jet, *Journal of Fluid Mechanics*, Vol. **33**, p.151.

Case No.	case1	case2	case3	case4
Breakup Length (cm), L_b	10	10	6.5	6.5
Fluid Initial Temp (°C), T_i	38.6	55.0	38.2	52.1
Background Air Temp (°C), T_a	20.0	20.2	20.2	20.1
D30 [mm]	2.243	2.245	2.019	2.069
Max. diameter [mm]	3.55	3.49	3.45	3.31
min. diameter [mm]	0.49	0.33	0.51	0.33
std deviation of drop size	0.6624	0.6590	0.6648	0.6664
variance	0.4387	0.4342	0.4419	0.4441
std error	0.0286	0.0278	0.0293	0.0275
no. of droplets measured in size	536	560	515	586
Tmean [°C]	35.51	49.56	35.35	48.53
Max. T [°C]	36.55	51.08	36.48	50.09
min. T [°C]	33.91	46.61	33.68	45.68
std deviation of drop T	0.3319	0.3528	0.4408	0.5814
variance	0.1102	0.3056	0.1943	0.3381
std error	0.0112	0.0216	0.0194	0.0262
no. of droplets measured in T	885	657	517	491
Vmean [m/s]	1.526	1.546	1.217	1.215
Max. Velocity [m/s]	1.83	2.26	1.53	1.85
min. Velocity [m/s]	1.10	1.25	0.90	0.95
std deviation of drop velocity	0.0816	0.0783	0.0686	0.0779
variance	0.0067	0.0061	0.0047	0.0061
std error	0.0035	0.0033	0.0030	0.0033
no. of droplets measured in V	532	552	510	569

Table I. The statistic information of droplet size, temperature, and velocity from measurements.

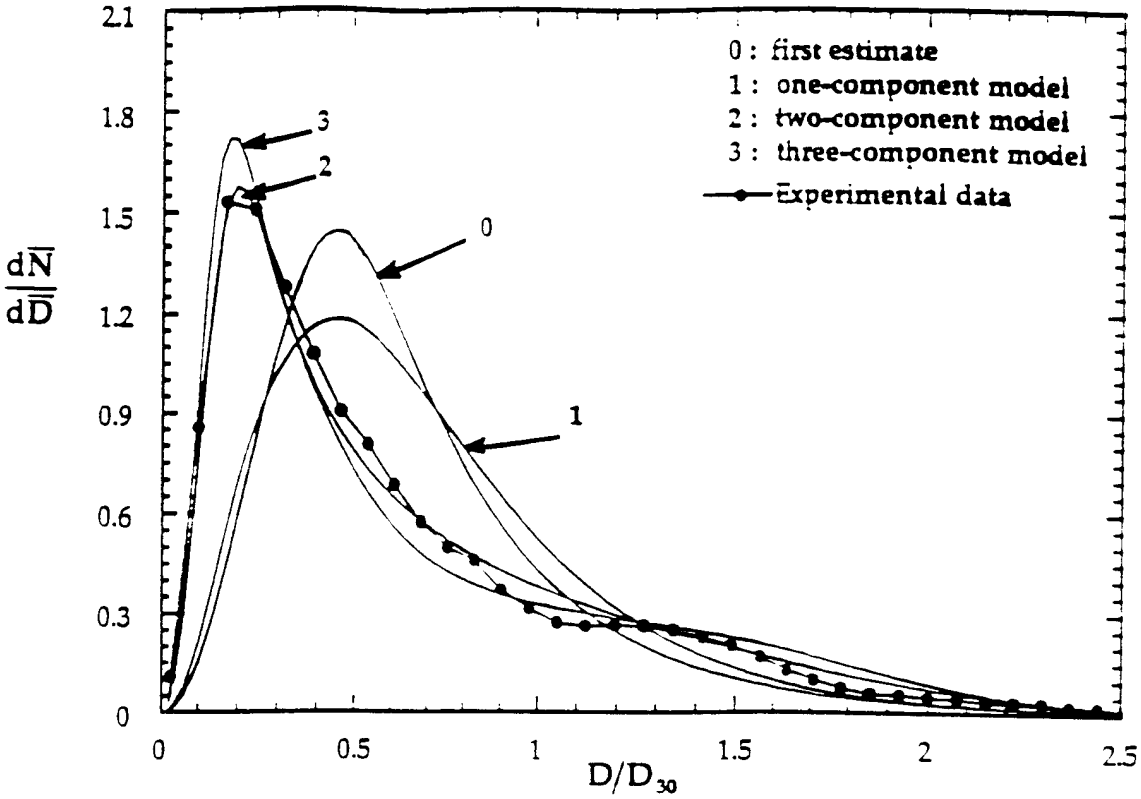

Figure 1. Comparison of droplet size distributions between experimental measurement and calculated results. In the three-component model the percentage of the third velocity component (tangential) in the total kinetic energy is 4%.

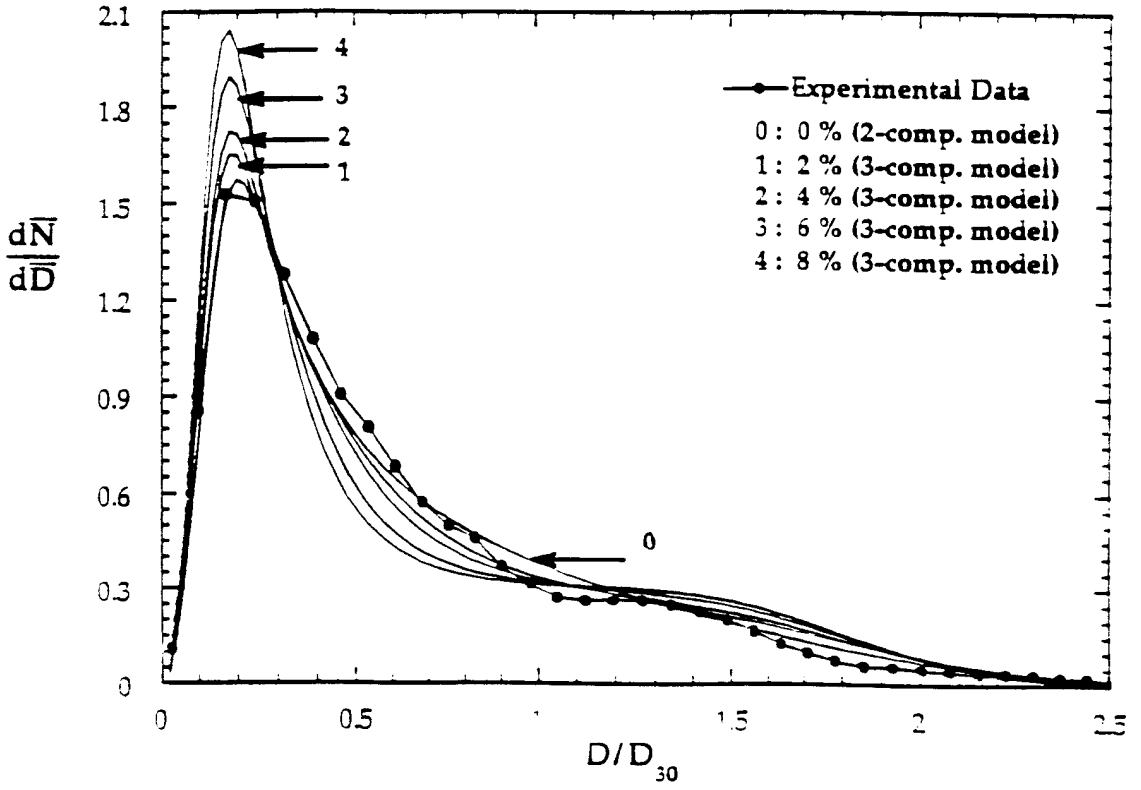

Figure 2. Droplet size distributions for various percentages of the third velocity component (tangential) in the total kinetic energy. Curve "2" is the same as curve "3" in figure 8(a).

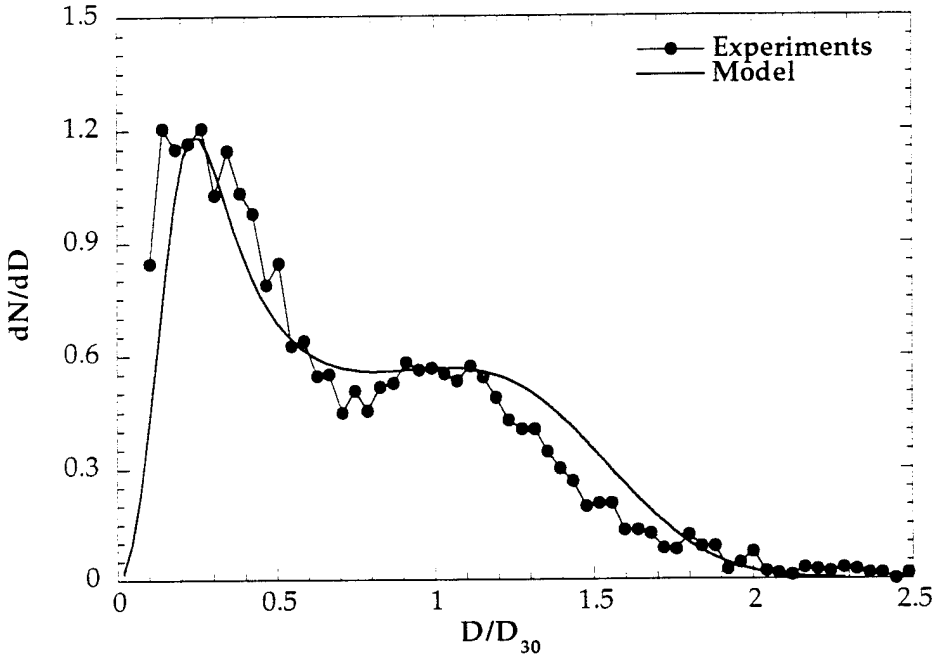

Figure 3. **Comparison of bi-modal droplet size distributions between model and experiment [Gupta et al., 1986]**

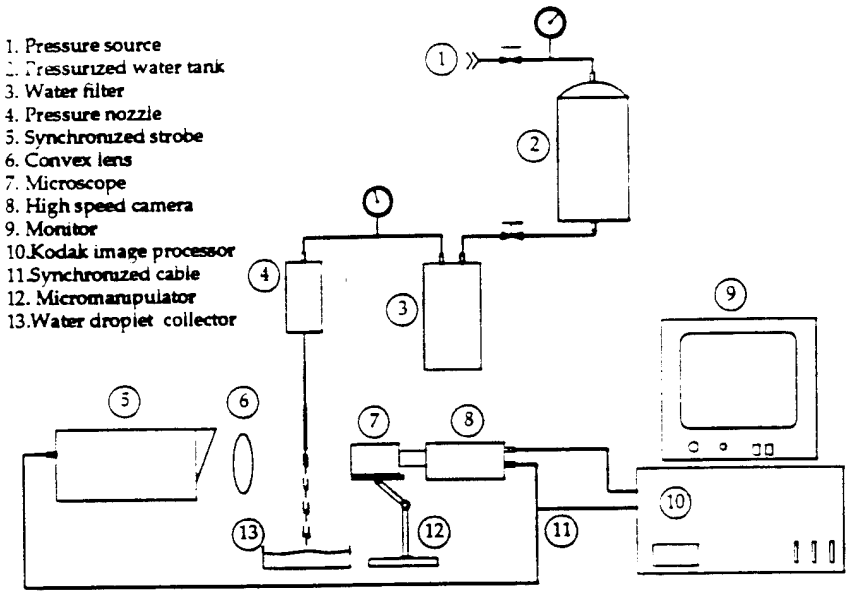

Figure 4. Schematic drawing of the droplet generator setup.

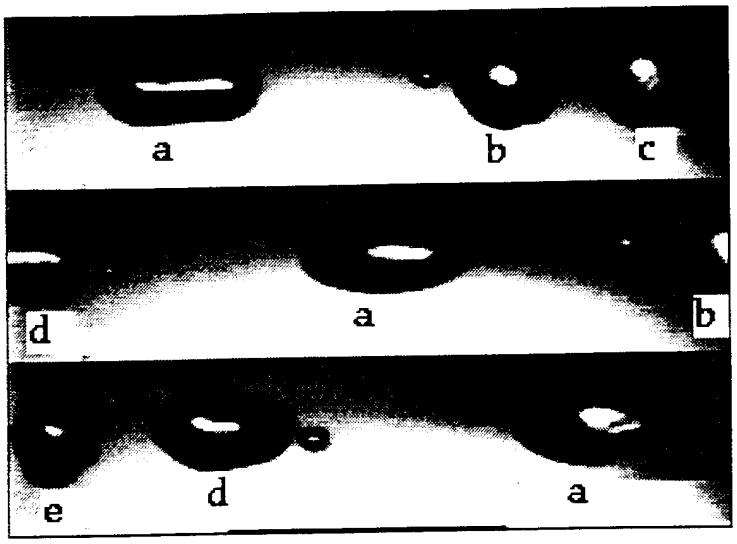

a

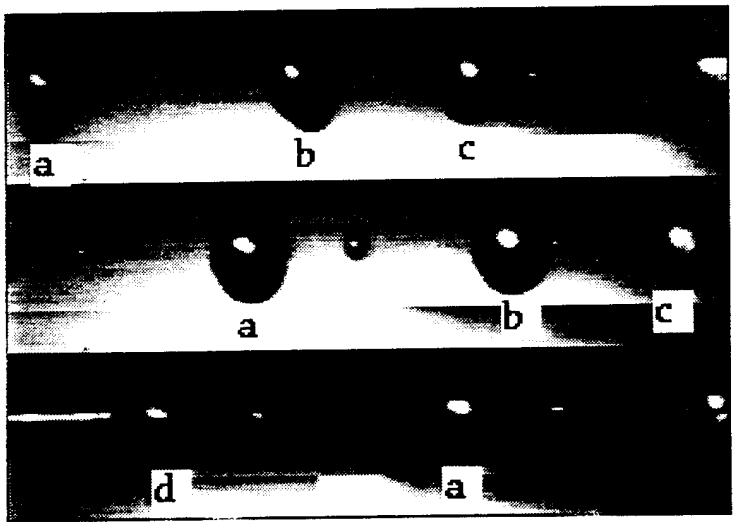

b

Figure 5. Typical images taken with the Ektapro Motion Analyzer 10 cm from nozzle.

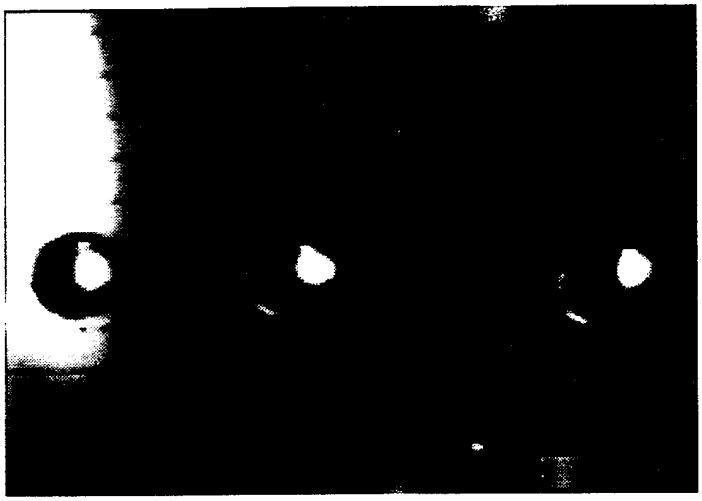

Figure 6. Typical image taken with the Ektapro Motion Analyzer 10 cm from nozzle.

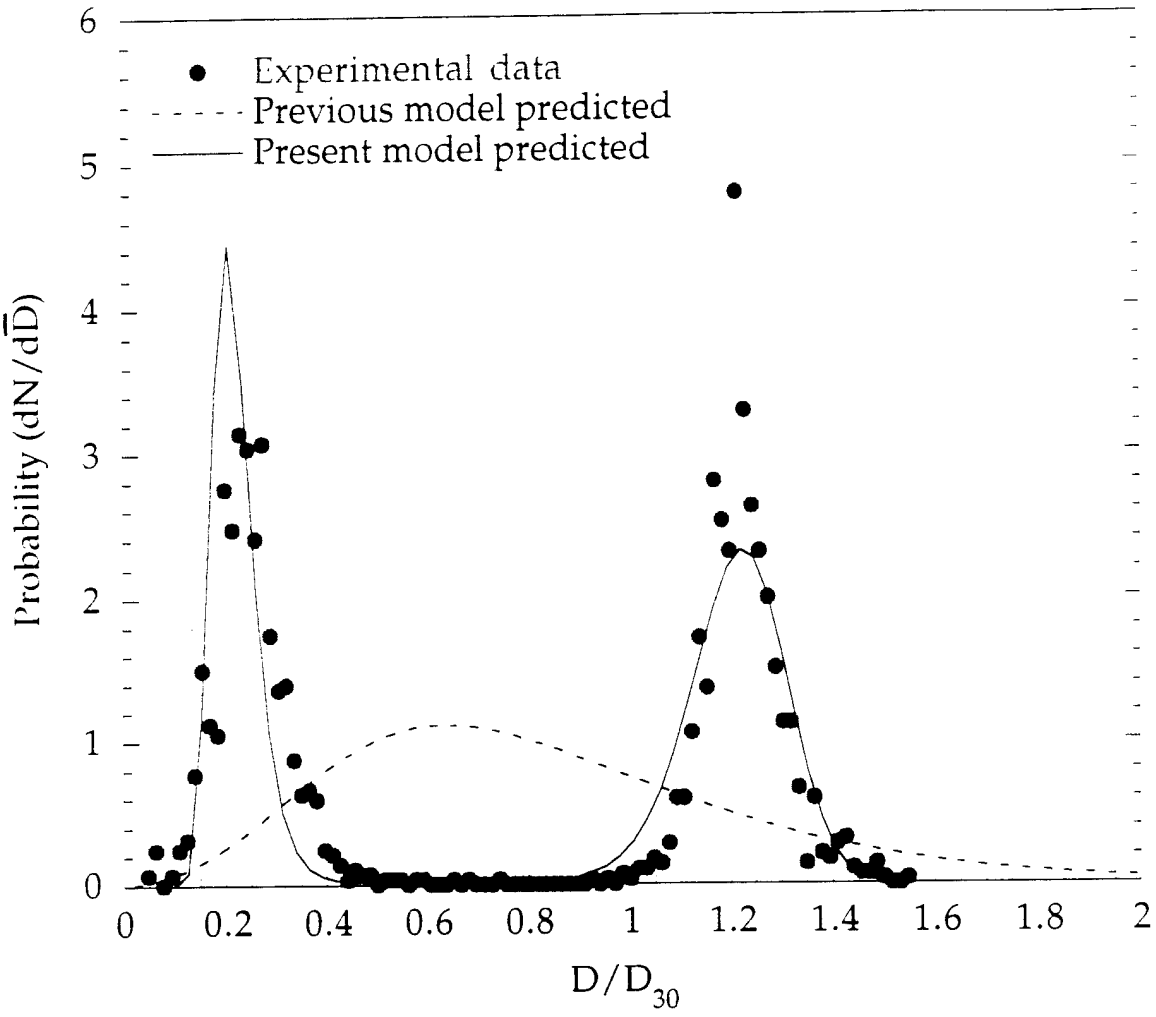

Figure 7. Comparison between experimental and predicted droplet size distributions.

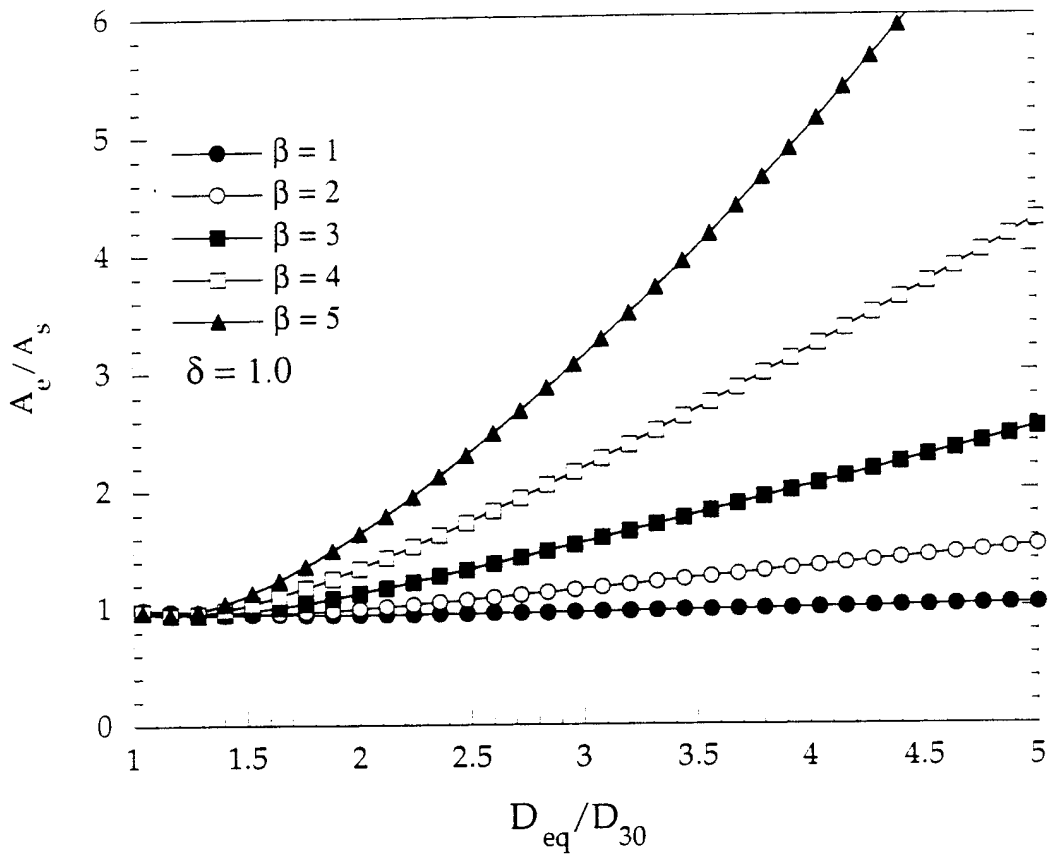

Figure 8. A plot of A_e/A_s versus D_{eq}, where A_e is the area of a prolate spheroid, and A_s is the area of a sphere having the same volume. a and b are the major and minor axes of the spheroid, and $a / b = \delta D_{eq}^{\beta}$.

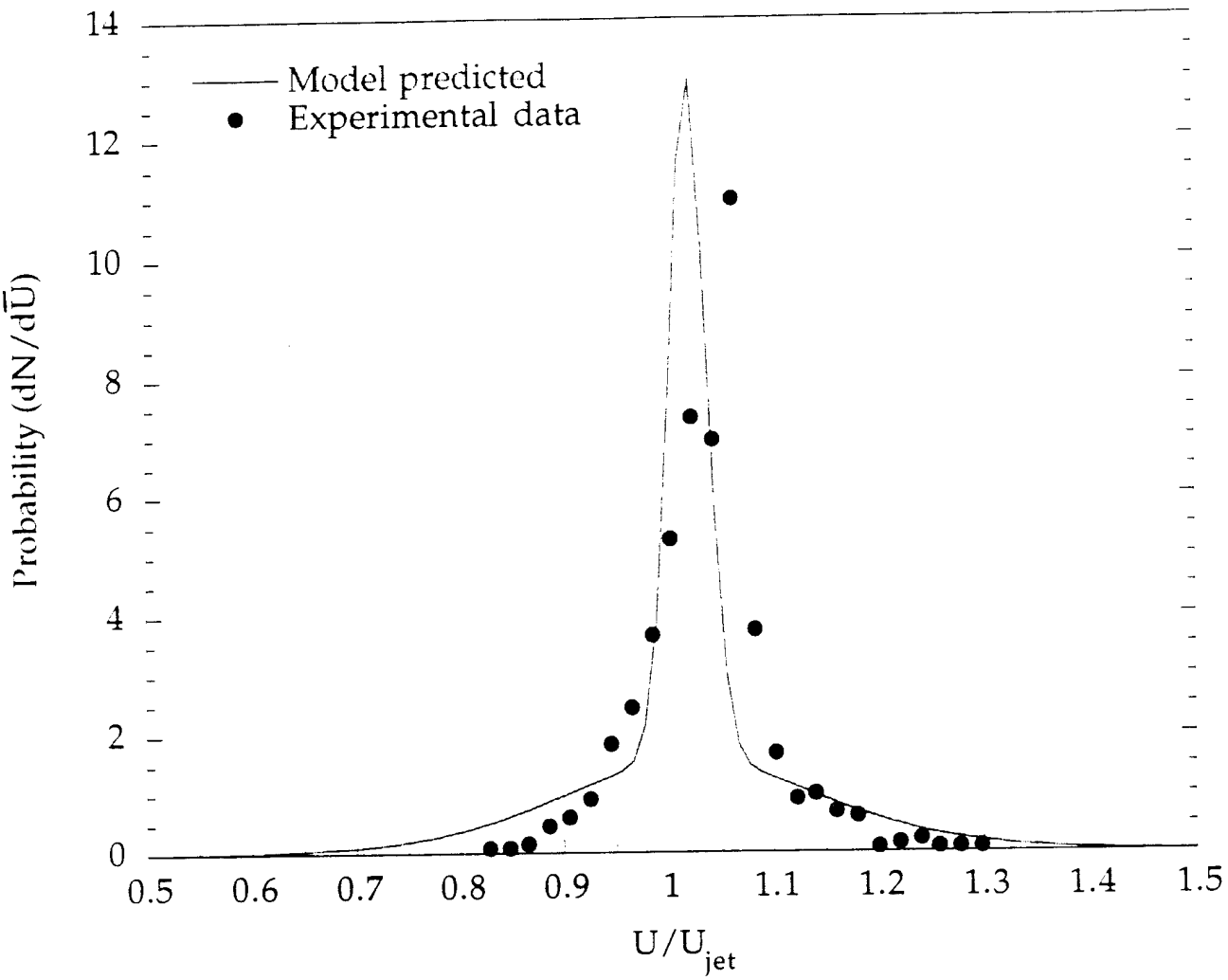

Figure 9. Comparison between experimental data and predicted droplet velocity distribution.

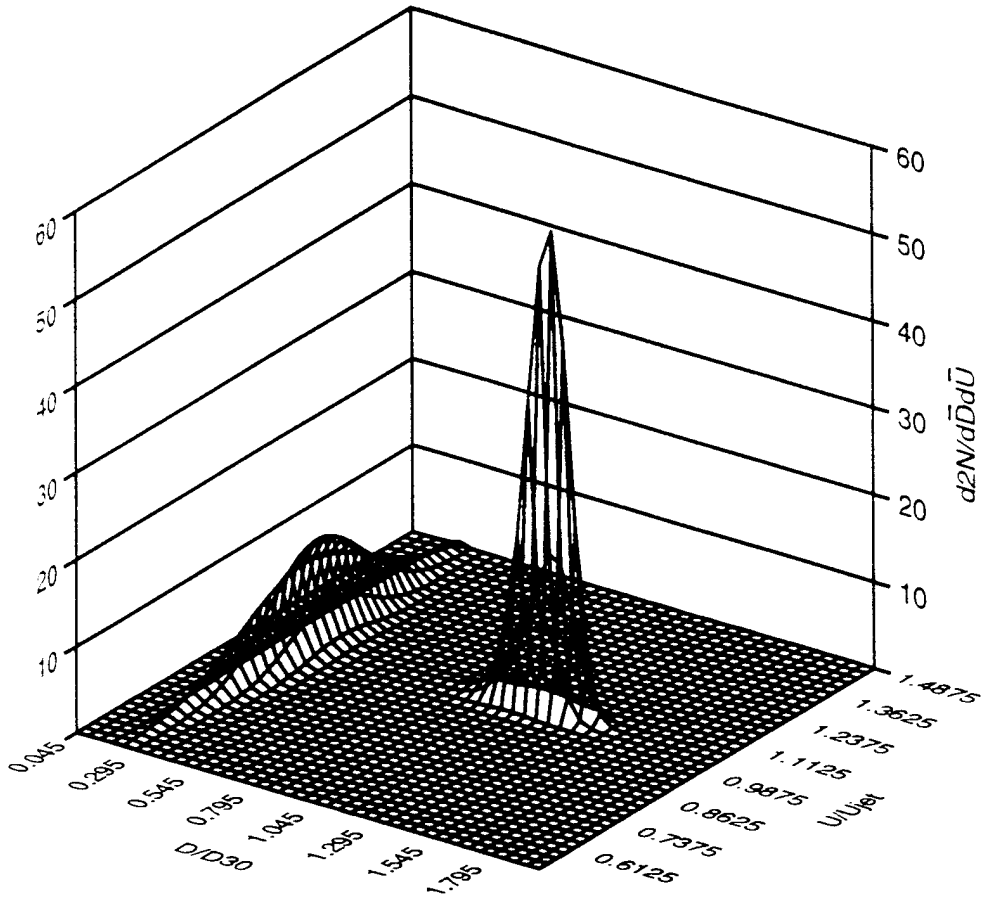

Figure 10. Three-dimensional plot of predicted joint probability distribution function.

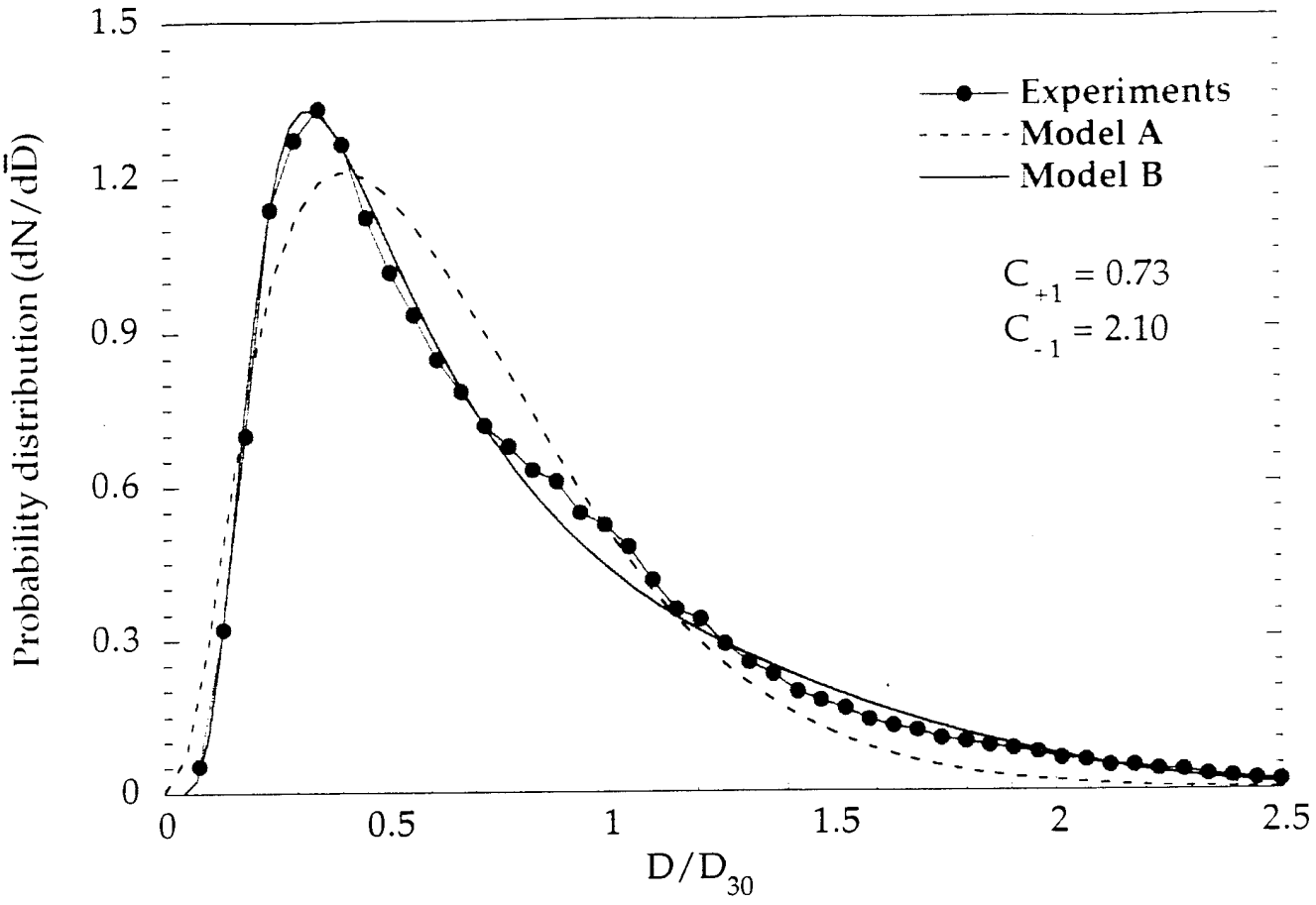

Figure 11. Plot of computed and measured droplet size distribution from a pressurized atomizer.

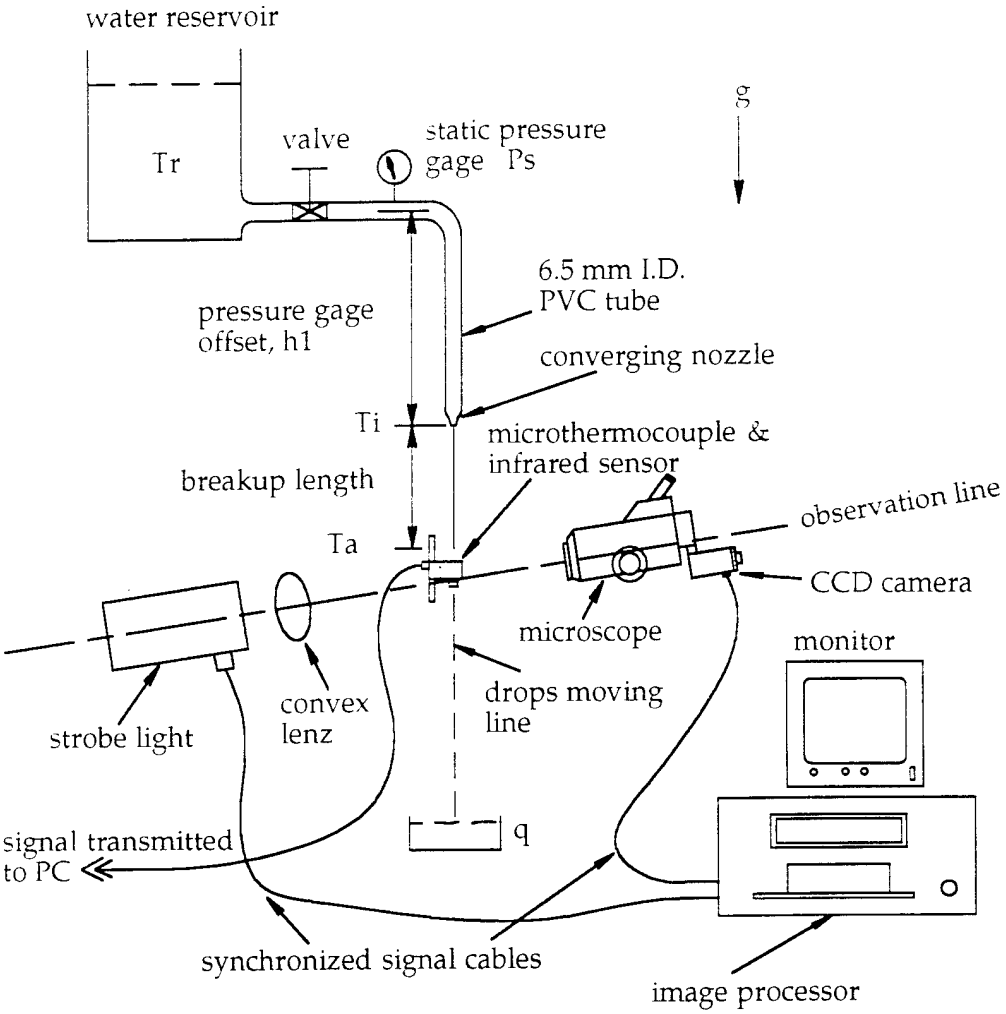

Figure 12. Schematic drawing for droplet temperature measurements.

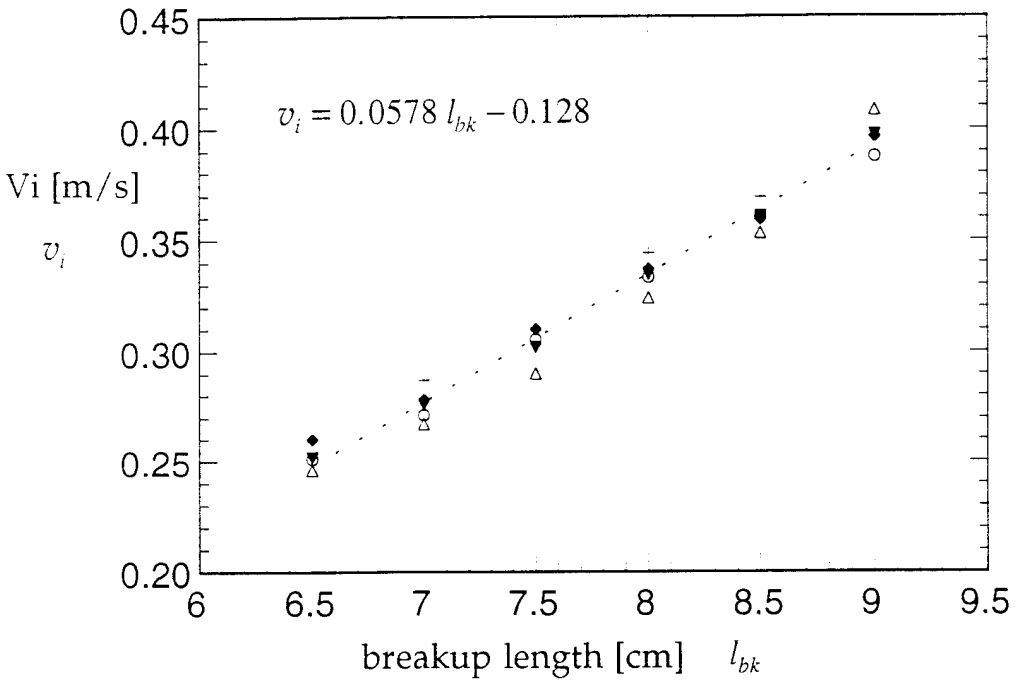

Figure 13. The effect of initial velocity on breakup length for a cylindrical liquid jet from a converging nozzle (Dexit=2.16 mm)

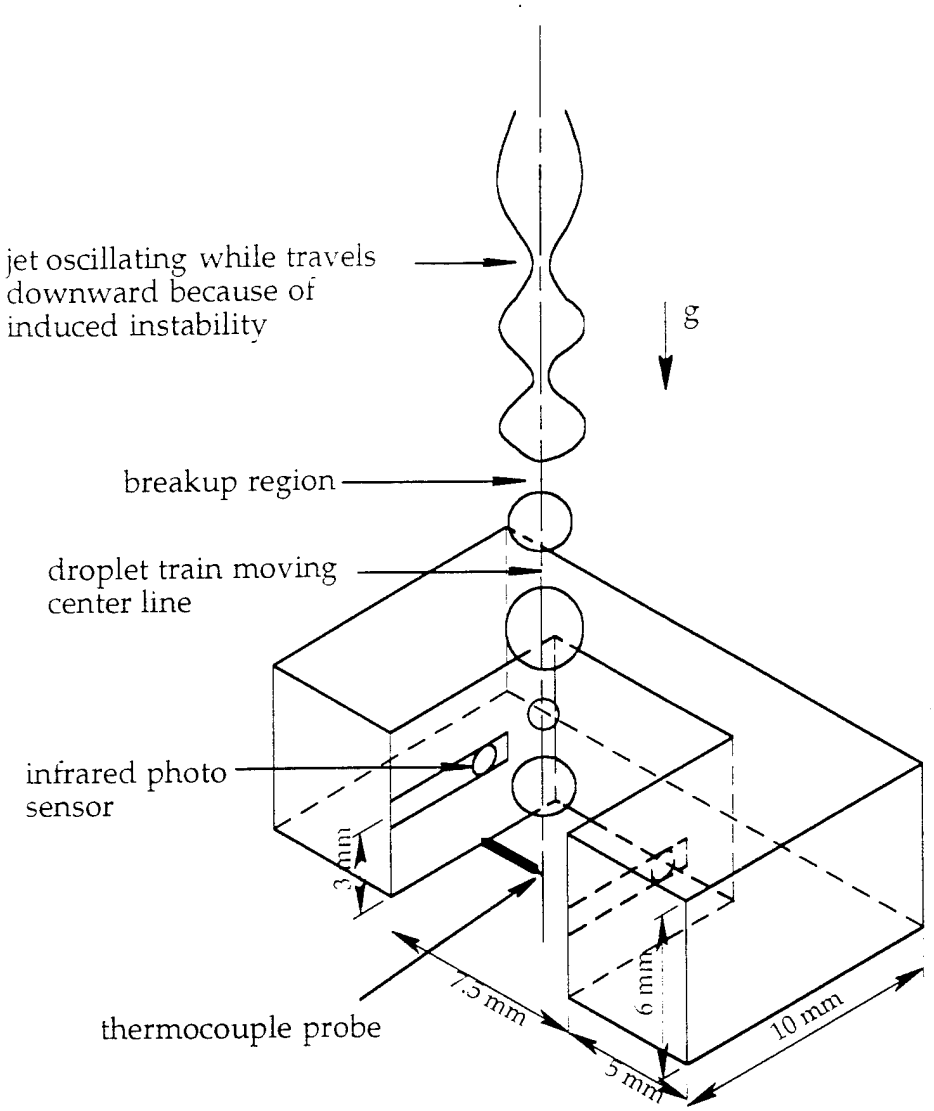

Figure 14. Schematic drawing shows the method of measuring droplet temperature of a cylindrical liquid jet by employing the infrared photo sensor and fast-response thermocouple.

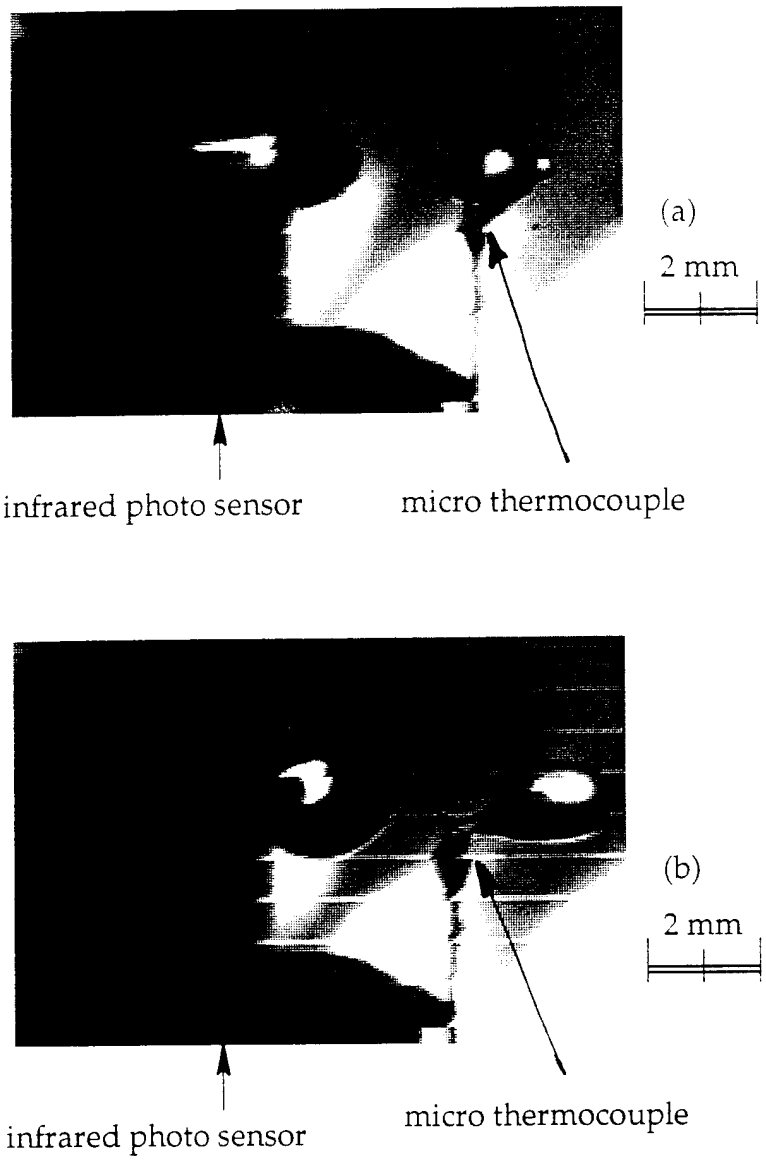

Figure 15. Droplets travel through the micro thermocouple :
(a) droplet is about to leave the thermocouple.
(b) droplet is leaving the thermocouple with a tail.

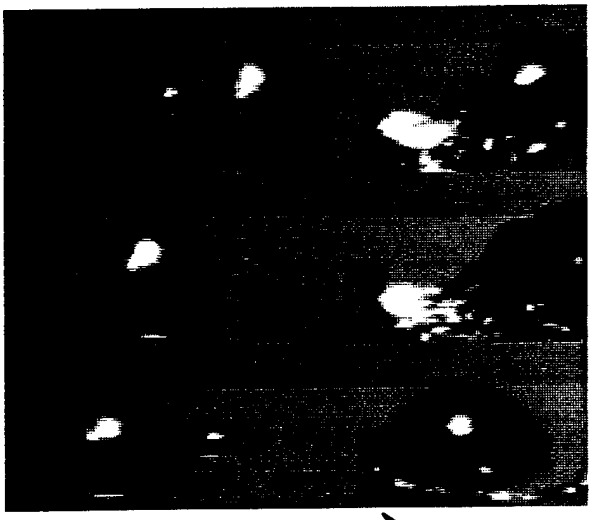

(a)

ball-head thermocouple

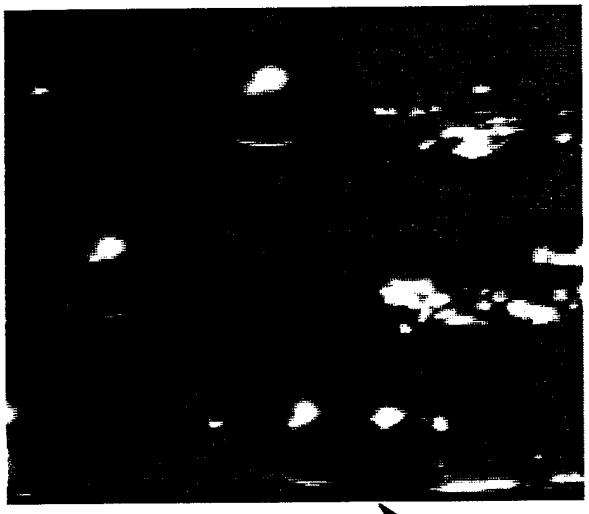

(b)

ball-head thermocouple

Figure 16. The detailed evolution of droplets travel through a ball-head thermocouple, recorded at 1500 pictures per second, the diameter of the thermocouple head is 0.12 mm

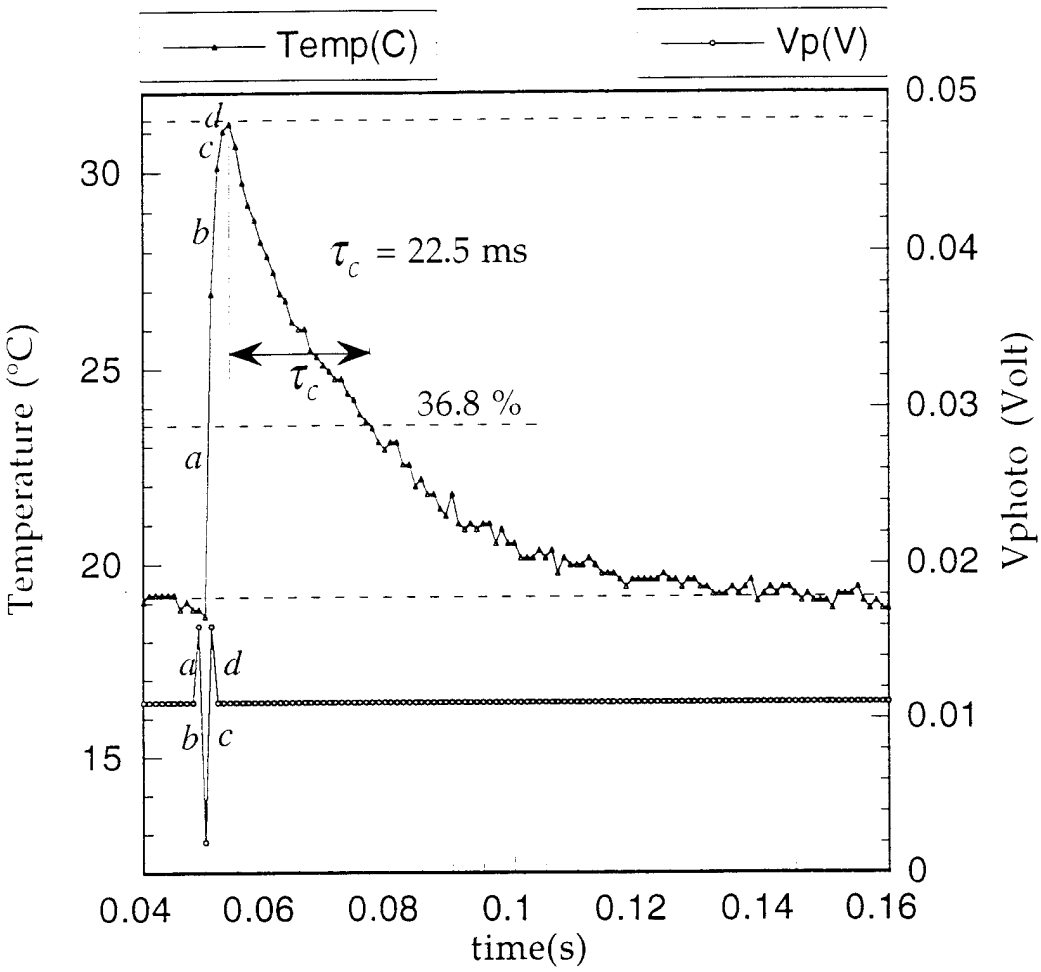

Figure 17. Calibration of thermocouple dynamic response by measuring dripping flow (8 drops/sec), Ti=32 °C, Tair=18 °C, sampling rate=1 kHz (single drop), cooling time constant= 22.5 ms

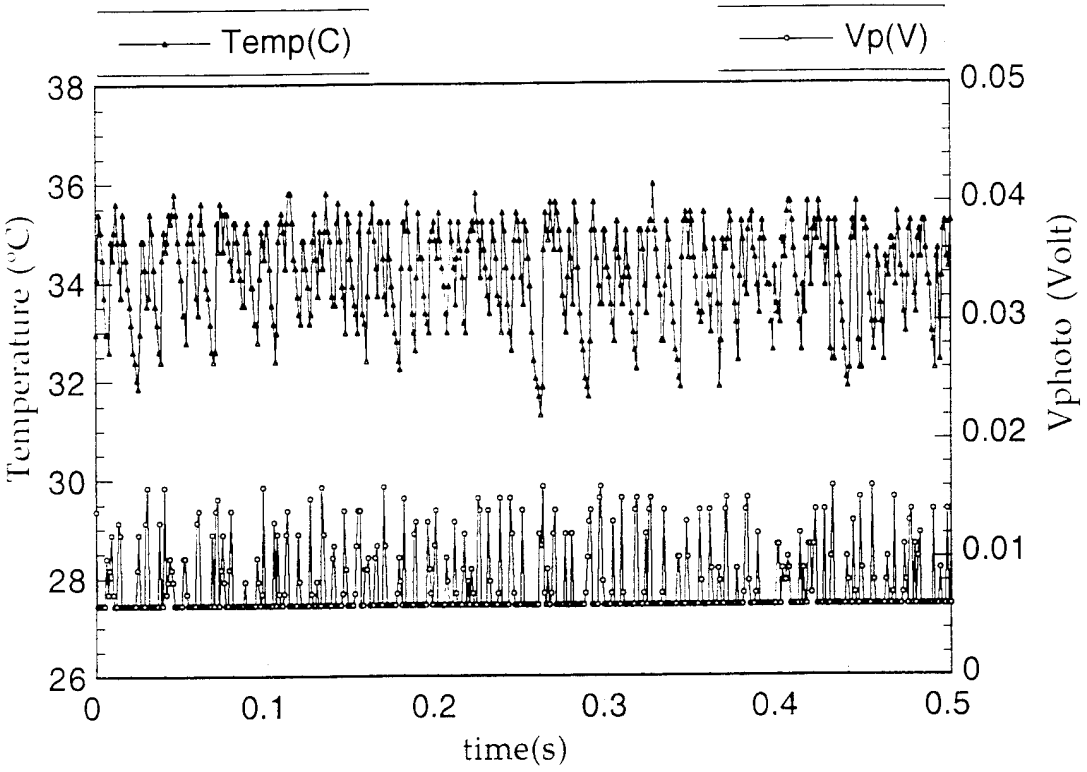

Figure 18. Typical droplet temperature measurement of a cylindrical liquid jet from a converging nozzle, Ti=38.6 °C,Tair=20.1 °C, q=93.5 ml/m, sampling rate=1 kHz (showing 0.5 second of measurements)

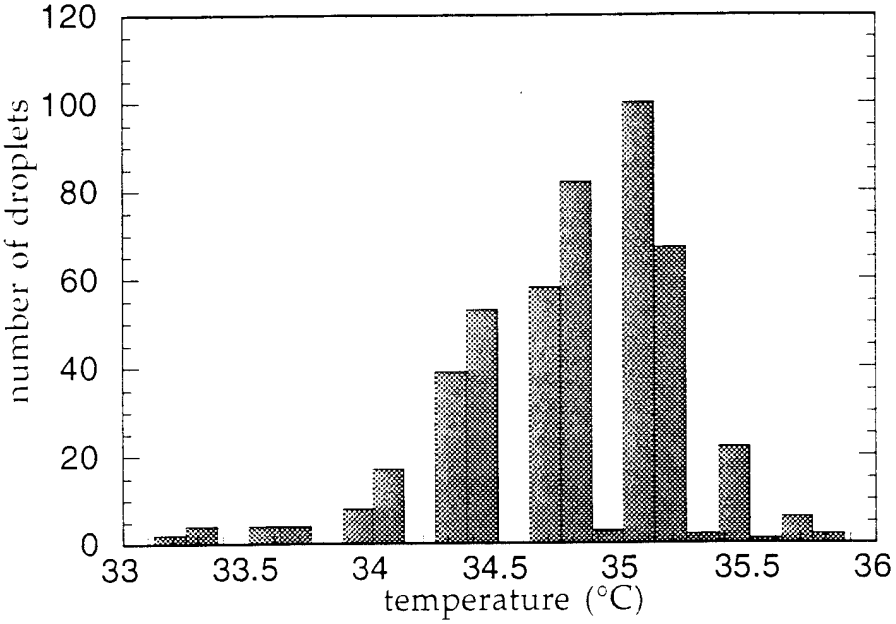

(a) typical droplet temperature distribution (raw data)

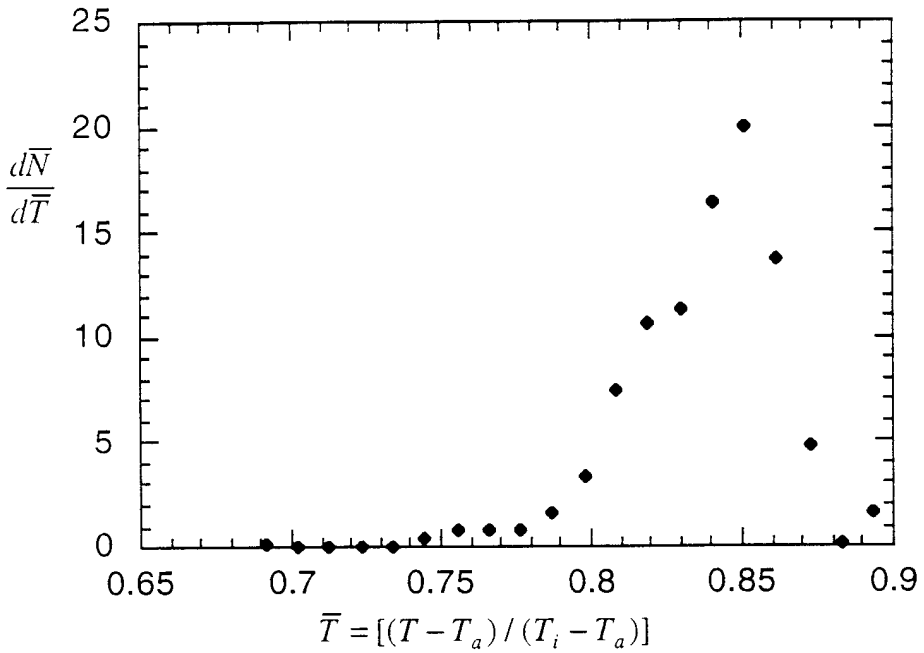

(b) normalized droplet temperature distribution

Figure 19. Experimental droplet temperature distribution at Ti=37.6 °C, Tair=20. °C, Lbk=10 cm, q=1.48 ml/sec

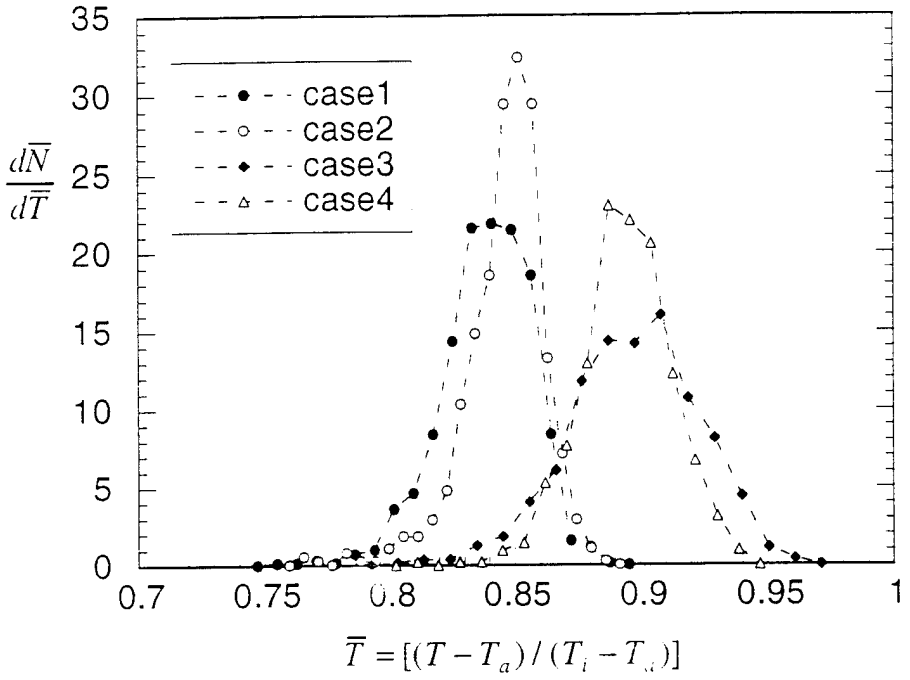

Figure 20. Experimental droplet temperature distribution of the cylindrical liquid jet from a converging nozzle

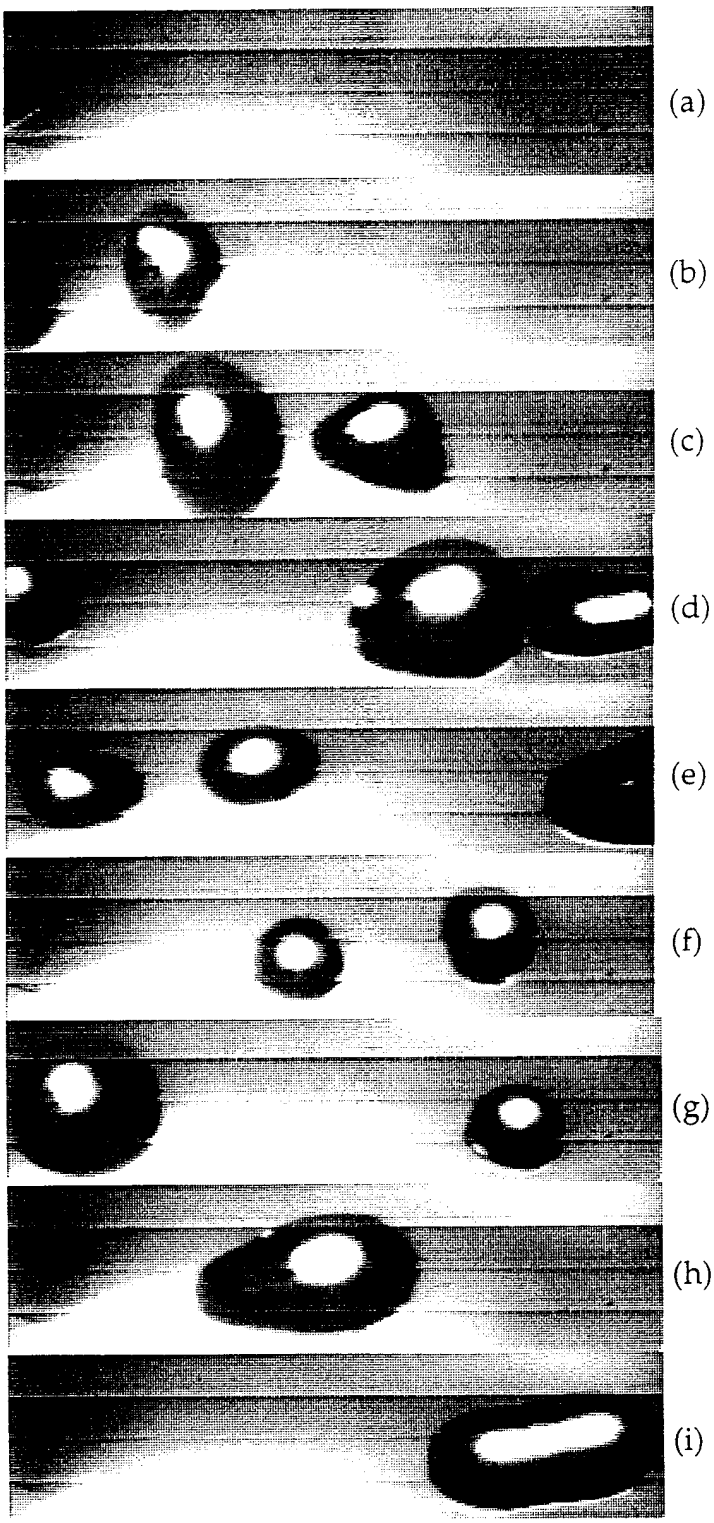

Figure 21. Droplet motion recorded in sequence at 12.5 cm below the exit of the nozzle at a framing rate of 375 pictures per second, breakup length=10 cm, Ti=38.6 °C, Ta=20.0 °C, q=1.55 ml/sec, droplets moving from left to right, total 5 droplets observed

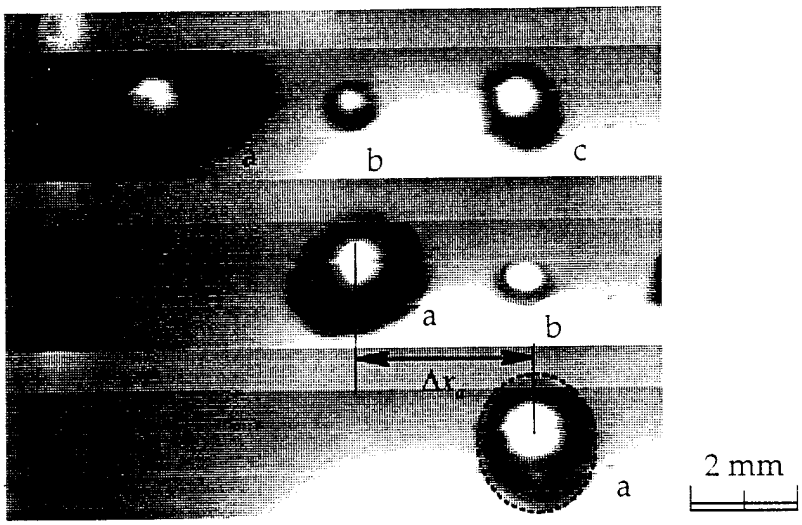

Figure 22. Droplet motion recorded in sequence at 9.0 cm below the exit of the nozzle at the rate of 375 pictures per second, breakup length=6.5 cm, Ti=38.2 °C, Ta=20.2 °C, q=0.90 ml/sec, droplets moving from left to right, Da=2.49 mm, Db=0.98 mm, Dc=1.68 mm, Va=1.23 m/sec, Vb=1.21 m/sec, and Vc=1.19 m/sec

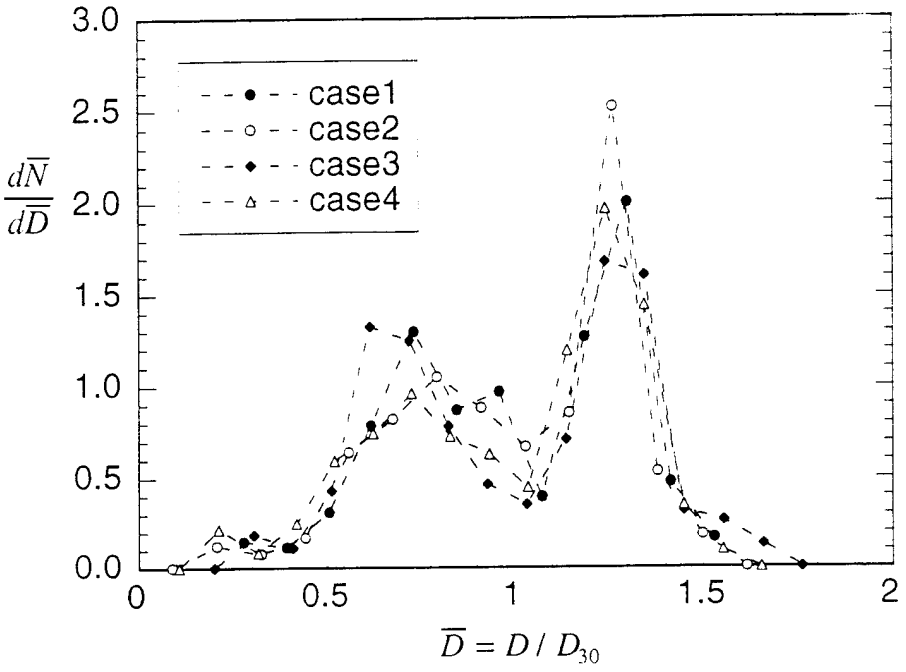

Figure 23. Experimental droplet size distribution of the cylindrical liquid jet from a converging nozzle

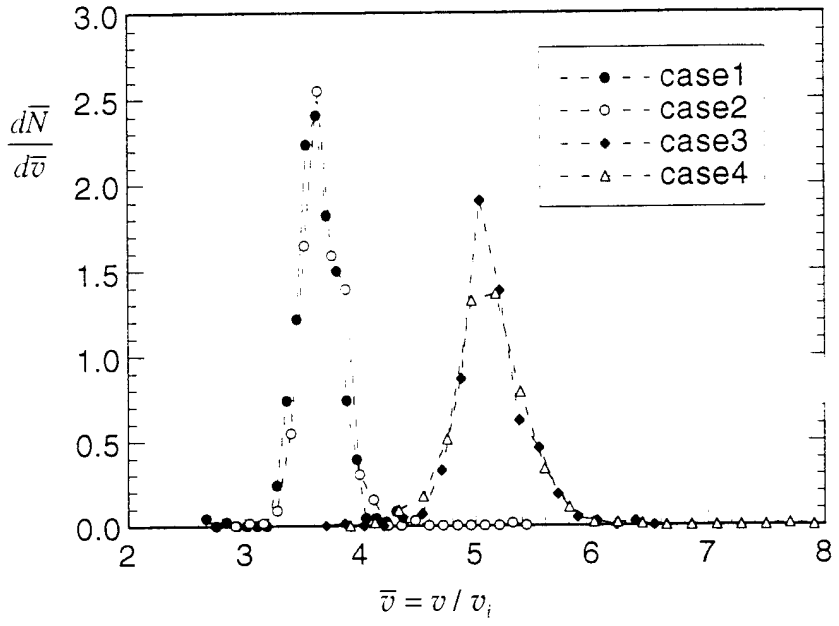

Figure 24. Experimental droplet velocity distribution of the cylindrical liquid jet from a converging nozzle

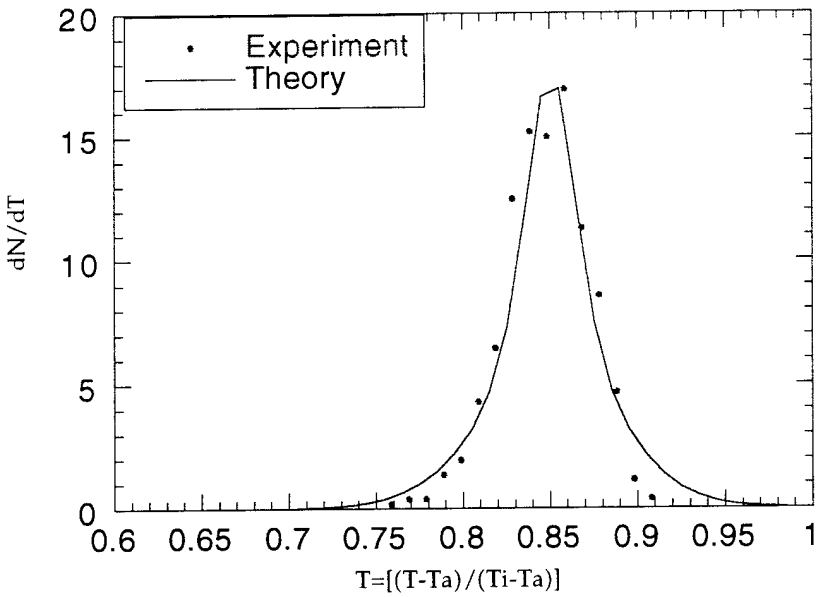

Figure 25. Droplet temperature distribution of cylindrical liquid jet from a converging nozzle.